Reciprocal interaction between mesenchymal stem cells and transit amplifying cells regulates tissue homeostasis

Junjun Jing[1,2], Jifan Feng[1], Jingyuan Li[1], Hu Zhao[1], Thach-Vu Ho[1], Jinzhi He[1,2], Yuan Yuan[1], Tingwei Guo[1], Jiahui Du[1], Mark Urata[1], Paul Sharpe[3], and Yang Chai[1*]

1. Center for Craniofacial Molecular Biology, University of Southern California, Los Angeles, CA 90033, USA

2. State Key Laboratory of Oral Diseases, National Clinical Research Center for Oral Diseases, West China Hospital of Stomatology, Chengdu, Sichuan, 610041, China

3. Department of Craniofacial Development and Stem Cell Biology, Dental Institute, Kings College London, London SE1 9RT, UK

*Corresponding author:
Yang Chai, DDS, PhD
University Professor
Center for Craniofacial Molecular Biology
University of Southern California
2250 Alcazar Street – CSA 103
Los Angeles, CA 90033
Phone number: 323-442-3480
ychai@usc.edu

Key words: mesenchymal stem cells, transit amplifying cells, cell interaction, homeostasis

Short title: Bi-directional interaction between MSCs and TACs

Abstract

Interaction between adult stem cells and their progeny is critical for tissue homeostasis and regeneration. In multiple organs, mesenchymal stem cells (MSCs) give rise to transit amplifying cells (TACs), which then differentiate into different cell types. However, whether and how MSCs interact with TACs remains unknown. Using the adult mouse incisor as a model, we present *in vivo* evidence that TACs and MSCs have distinct genetic programs and engage in reciprocal signaling cross-talk to maintain tissue homeostasis. Specifically, an IGF-WNT signaling cascade is involved in the feedforward from MSCs to TACs. TACs are regulated by tissue-autonomous canonical WNT signaling and can feedback to MSCs and regulate MSC maintenance via Wnt5a/Ror2-mediated non-canonical WNT signaling. Collectively, these findings highlight the importance of coordinated bi-directional signaling interaction between MSCs and TACs in instructing mesenchymal tissue homeostasis, and the mechanisms identified here have important implications for MSC-TAC interaction in other organs.

Introduction

The regulation of tissue homeostasis is a fundamental function of adult stem cells. Once stem cells leave their niche, they commit to a more restricted lineage and/or differentiate into specific cell types. In many tissues and organs, during this process stem cells give rise to transit amplifying cells (TACs), an undifferentiated progenitor population[1,2,3]. TACs function as transient but indispensable integrators of stem cell niche components[4,5,6]. Several independent studies have revealed that stem cells actively interact with their progeny during tissue homeostasis and regeneration[7,8,9]. For example, regulatory feedback from TACs may instruct stem cells to replenish downstream lineages and serve to coordinate stem cell self-renewal during tissue homeostasis and regeneration of adult ectodermal organs[8]. Another study reported that, in the airway epithelium, the parent epithelial stem cells relay Notch signaling to regulate differentiation in their daughter secretory progenitor cells[9]. To date, however, these pioneering studies have exclusively focused on ectodermal organs, and it remains unknown how mesenchymal stem cells (MSCs) interact with TACs to maintain tissue homeostasis.

The mouse incisor provides an ideal model for studying the interaction of MSCs and TACs because the stem cells and their niche are retained throughout the mouse's life to support continuous incisor growth, and the anatomical locations of the dental pulp stem cells and TAC populations have recently been clearly defined[10,11,12,13]. The mouse incisor is comprised of an outer layer of enamel with dentin underneath, and an inner chamber of dental pulp that contains vasculature and nervous tissue. The epithelial and mesenchymal compartments of the incisor both replenish all of their cells within the course of a month[12]. The continuous turnover of mesenchymal tissue is supported by MSCs in the proximal region of the mouse incisor. Our previous study demonstrated that quiescent Gli1+ dental pulp cells are typical MSCs in the mouse incisor and they generate TACs that can be

found in the immediately adjacent region[12]. Gli1+ MSCs can continuously populate the incisor mesenchyme throughout the animal's lifetime[12]. TACs actively proliferate, giving rise to committed preodontoblasts, terminally differentiated odontoblasts, and dental pulp cells. Recent studies have also identified that polycomb repressive complex 1 (PRC1) regulates the TACs via WNT/β-catenin signaling, and that Axin2 expression identifies the TAC population, which is unable to maintain itself through self-renewal[10].

In this study, we took advantage of specific molecular markers that allowed us to identify and target either MSCs or TACs in the adult mouse incisor *in vivo* and we found that MSCs and TACs have distinct genetic programs that may help them define their *in vivo* identities and interact with each other. We learned that MSCs feedforward to TACs through an IGF-WNT signaling cascade and the control of TAC fate depends on tissue-autonomous canonical WNT signaling. In parallel, TACs produce Wnt5a, which provides feedback to MSCs via Ror2-mediated non-canonical WNT signaling. Our study provides *in vivo* evidence of the reciprocal interaction between MSCs and TACs in mesenchymal tissue homeostasis and highlights the molecular regulatory mechanism that governs this interaction. The mechanisms identified in this study could potentially apply to other organs, such as long bone, where MSC and TAC interaction is not well understood but may also be crucial for maintaining tissue homeostasis and regeneration.

Results

Anatomical and molecular identities of MSCs and TACs in the mouse incisor

In order to study the interaction between MSCs and TACs, we first confirmed their *in vivo* locations using recently published markers. In addition to Axin2, TACs are also identifiable by their active proliferation status[12], consistent with our findings that Axin2+ and Ki67+ populations both reside in the TAC region (Figures 1A and 1B). Therefore, we used both Axin2 and Ki67 as TAC markers. Gli1 is a known dental MSC marker in the adult mouse incisor[12]. Our data clearly indicate that Gli1+ MSCs and TACs are mutually exclusive cell populations in adult incisors (Figures 1C and 1D), consistent with our previous findings[12]. This allowed us to use *Gli1-CreER^{T2}* and *Axin2-CreER^{T2}* to target MSCs and TACs in the mouse incisor, respectively. The close proximity between the MSCs and TACs in the mouse incisor suggests a physical environment conducive of cell-cell interaction between these two populations (Figure 1E).

IGF ligand and binding proteins are highly enriched in MSCs

Identifying genetic signatures of MSCs and TACs is critical to understanding the genetic programs involved in establishing and maintaining their identities as well as uncovering how these two populations interact. To identify genetic profiles of MSCs and TACs, we used laser capture microdissection to collect the MSC region from *Gli1-CreER^{T2};Rosa26$^{<fs\text{-}tdTomato>}$* mice and the TAC region from *Axin2-CreER^{T2};Rosa26$^{<fs\text{-}tdTomato>}$* mice shortly after labelling, followed by unbiased RNA sequencing analysis of these samples. We found that specific signaling pathways were preferentially enriched in either TACs or MSCs based on Ingenuity Pathway Analysis (IPA, QIAGEN). We first analyzed the signaling enriched in TACs. As expected for Axin2+ TACs, WNT/β-catenin signaling was one of the top enriched pathways. Cell cycle regulation signaling

was also highly active, consistent with the high proliferative activity of TACs. Moreover, mTOR and EIF2 signaling, which are both important for cell proliferation, were also enriched in TACs (Figure 2A). We focused on IGF signaling based on previous reports that it plays a role in stem cell homeostasis[14,15]. We investigated the ligands and receptors of IGF signaling that were found among the significantly differentially expressed genes between incisor MSCs and TACs identified by RNA sequencing. Although IGF signaling was highly active in TACs, we found that IGF signaling molecules including IGF binding protein (Igfbp3) and the IGF ligand, insulin-like growth factor 2 (Igf2), were all highly enriched in MSCs (Figure 2B). RNAscope *in situ* hybridization confirmed that *Igfbp3* was highly expressed in MSCs outside of the TAC region and dental follicle *in vivo* (Figure 2C-2D), and *Igf2* also appeared to be highly expressed in a similar pattern (Figures 2E-2F). Interestingly, consistent with the pathway analysis (Figure 2A), expression of *Igf1r*, an IGF receptor, was detectable in the mouse incisor mesenchyme overlapping the TAC region (Figures 2G-2H), indicating that MSC- and dental follicle-derived IGF signals may affect TAC fate through the IGF signaling pathway.

Inactivation of IGF signaling leads to diminished TACs and compromised WNT signaling in the incisor mesenchyme

In order to investigate the potential role of IGF signaling in MSC-TAC interaction, we generated *Axin2-CreER^{T2};Igf1r$^{fl/fl}$* mice, in which *Igf1r* could be deleted in Axin2+ TACs via tamoxifen induction. We found that the number of TACs in the mesenchyme was diminished three weeks after induction (Figures 3C-3E), indicating that IGF signaling is critical for TAC proliferation. In addition, the dentin became thicker in *Axin2-CreER^{T2};Igf1r$^{fl/fl}$* mice (Figure 3A-3B), indicating premature differentiation of TACs, suggesting that IGF signaling pathway may regulate TAC fate through balancing proliferation and differentiation. We found that the number of TACs in the

incisor epithelium of *Axin2-CreER^{T2};Igf1r$^{fl/fl}$* mice was also reduced three weeks after induction (Figure 3C-3D), suggesting epithelial-mesenchymal interaction occurred at this stage. Because *Axin2-CreER^{T2}* is highly active in the TAC region of the incisor mesenchyme but not the epithelium, we hypothesized that the effect from the mesenchyme is primary. In order to test whether loss of *Igf1r* in Axin2+ TACs in the incisor mesenchyme was indeed the primary cause of the TAC loss, we analyzed the change of TACs in *Axin2-CreER^{T2};Igf1r$^{fl/fl}$* incisors at an earlier time point and found that the number of TACs in the mesenchyme was already reduced whereas differentiation (indicated by *Dspp,* which is a marker for odontoblasts) was enhanced one week after induction (Figure 3-figure supplement 1). However, the number and differentiation status of TACs in the incisor epithelium (indicated by Amelx, which is a marker for ameloblasts) remained unchanged in *Axin2-CreER^{T2};Igf1r$^{fl/fl}$* mice at this time point (Figure 3-figure supplement 1), suggesting that epithelial-mesenchymal interaction occurs later and the effect from the incisor mesenchyme is primary. Moreover, we found that Axin2 expression was reduced in TACs, suggesting that canonical WNT signaling is likely to be downstream of IGF signaling in the regulation of TACs (Figures 3F and 3G). Consistent with reduced Axin2 expression, we found that other WNT downstream genes such as c-Myc and active β-catenin were also downregulated (Figure 3-figure supplement 2). Therefore, we concluded that MSCs and the dental follicle secrete Igf2 ligand to regulate TACs through an IGF-WNT signaling cascade (Figure 3H). We found that the phenotype in *Axin2-CreER^{T2};Igf1r$^{fl/fl}$* incisors persisted five months after induction, suggesting disturbed tissue homeostasis of the incisor at later stages (Figure 3-figure supplement 3).

WNT signaling molecules are enriched in TACs but not MSCs

Previous studies have shown that WNT signaling is important for TAC regulation[10]. Due to the close anatomical proximity of MSCs and TACs, we further analyzed whether WNT ligands are

secreted by MSCs in a paracrine manner or by TACs in an autocrine manner. Surprisingly, TACs, not MSCs, seem to be the main source of both canonical and non-canonical WNT ligands (Wnt10a and Wnt5a, respectively) (Figure 4A). Wnt10a was detectable in the TAC region in the mesenchyme, although it was also expressed in odontoblasts and the epithelium (Figures 4B and 4C). Wnt5a was also highly expressed in TACs as well as in odontoblasts and in the dental mesenchyme, but excluded from the MSC region in the incisor (Figures 4D and 4E). To test whether any other WNT ligands were expressed in MSCs or TACs, we assessed the expression patterns of the 17 other WNT ligands. None were enriched in either MSCs or TACs: some were only expressed in the epithelium but not in the mesenchyme, such as Wnt3a and Wnt4, whereas others were undetectable in both the epithelium and the mesenchyme (Figure 4-figure supplement 1). This result suggests that both canonical and non-canonical WNTs in the incisor mesenchyme are mainly TAC-derived. To search for the cells that are responsive to the WNTs, we analyzed enriched pathways in both TACs and MSCs. Interestingly, canonical WNT/β-catenin signaling was enriched in TACs (Figure 2A) whereas non-canonical NFAT signaling was enriched in MSCs (Figure 4F).

Loss of WNT signaling in odontoblasts has no effect on MSCs or TACs

To test whether WNT signaling in odontoblasts has an effect on MSCs or TACs, we generated *Dmp1-Cre;Wls*$^{fl/fl}$*;Gli1-LacZ* mice in which odontoblasts are unable to secrete the WNT ligand. We found that there was no significant difference between *Gli1-LacZ* and *Dmp1-Cre;Wls*$^{fl/fl}$*;Gli1-LacZ* mice in the number of TACs and MSCs, suggesting that loss of WNT signaling in odontoblasts has no effect on MSCs or TACs (Figure 4-figure supplement 2).

Axin2+ TACs are regulated via tissue-autonomous canonical WNT signaling

In order to investigate the effect of the WNT ligand in Axin2+ TACs, we generated *Axin2-CreER^{T2};Wls$^{fl/fl}$;Gli1-LacZ* mice, in which Axin2+ cells are not able to secrete the WNT ligand. We confirmed that Wls was expressed in the TAC region of control mice, whereas it was undetectable in the TAC region of *Axin2-CreER^{T2};Wls$^{fl/fl}$;Gli1-LacZ* mice (Figure 4-figure supplement 3A-3B). Interestingly, we found that the *Axin2-CreER^{T2};Wls$^{fl/fl}$;Gli1-LacZ* mouse incisors were significantly shorter one month after tamoxifen induction (Figure 4-figure supplement 3C-3D), suggesting that loss of *Wls* affected their tissue turnover and homeostasis. More importantly, loss of *Wls* in Axin2+ cells resulted in a loss of TACs, as assessed by Ki67 staining (Figure 4-figure supplement 3E-3F). In order to confirm that TACs were indeed diminished, we also examined the expression of *Fgf10*, which is secreted by TACs in the mesenchyme[16,17], and found that *Fgf10* was greatly reduced in *Axin2-CreER^{T2};Wls$^{fl/fl}$;Gli1-LacZ* mice (Figure 4-figure supplement 3G-3H). In addition, in *Axin2-CreER^{T2};Wls$^{fl/fl}$;Gli1-LacZ* mice, there was a reduction of Gli1+ MSCs (Figure 4-figure supplement 3I-3L), indicating that TAC-derived WNT signaling may play a role in MSC maintenance. Therefore, TACs may secrete WNTs to regulate the fates of TACs and MSCs.

Axin2 is a readout of canonical WNT signaling. Consistent with the expression of Axin2 in TACs, we found that Lrp5, a canonical WNT receptor, was highly expressed in TACs (Figure 4-figure supplement 4A-4B), whereas Fzd2, Fzd4 and Fzd6 were almost undetectable in the incisor mesenchyme (Figure 4-figure supplement 4C-4H). These data suggest that Axin2+ TACs are regulated via tissue-autonomous canonical WNT signaling.

TACs feedback to MSCs via Wnt5a/Ror2-mediated non-canonical WNT signaling

Because Gli1+ MSCs were reduced in *Axin2-CreER^{T2};Wls$^{fl/fl}$;Gli1-LacZ* mice in which Axin2+ TACs are unable to secrete WNT ligands, we hypothesized that TAC-derived WNTs can act on MSCs via a paracrine mechanism. Interestingly, delayed molar development has been observed in *Wnt5a$^{-/-}$* mutant mice, consistent with the notion that Wnt5a-mediated non-canonical WNT signaling plays a role during tooth development[18], indicating that Wnt5a may play an important role in feedback from TACs to MSCs in the maintenance of incisor tissue homeostasis. To test our hypotheses, we generated *Axin2-CreER^{T2};Wnt5a$^{fl/fl}$;Gli1-LacZ* mice. We first examined the efficiency of Wnt5a deletion in *Axin2-CreER^{T2};Wnt5a$^{fl/fl}$* incisors and confirmed that Wnt5a was efficiently deleted in the TAC region of the mutant incisors three days after tamoxifen induction (Figure 5-figure supplement 1). We found that TACs were not affected in *Axin2-CreER^{T2};Wnt5a$^{fl/fl}$;Gli1-LacZ* mice three weeks after tamoxifen induction (Figures 5A-5C) but by that time the number of Gli1+ MSCs was already reduced in these *Wnt5a* mutants (Figures 5D-5H), suggesting that Wnt5a acts as a paracrine WNT ligand to regulate the maintenance of Gli1+ MSCs. We also used label retaining cells (LRCs), which serve as a hallmark of stem cells, to confirm the decrease of MSCs in the incisor of *Wnt5a* mutant mice. We found that loss of *Wnt5a* resulted in diminished LRCs in the MSC region in *Axin2-CreER^{T2};Wnt5a$^{fl/fl}$* mice (Figure 5-figure supplement 2). Thicker dentin and diminished TACs were observed in *Axin2-CreER^{T2};Wnt5a$^{fl/fl}$;Gli1-LacZ* mice at later stages (Figure 5-figure supplement 3), indicating disturbed homeostasis of the incisor after the disruption of TACs feedback to MSCs. To investigate the signaling mechanism of TAC feedback to MSCs, we examined the expression of Ror2, which serves as a key receptor for Wnt5a. We found that Ror2 was highly expressed in the MSC region of the incisor mesenchyme (Figures 6A), consistent with regulation of Gli1+ MSCs by Wnt5a-mediated non-canonical WNT signaling feedback through Ror2. In order to investigate the

function of Ror2-mediated non-canonical WNT signaling in the feedback from TACs to MSCs, we generated *Gli1-CreER^{T2};Ror2$^{fl/fl}$;Gli1-LacZ* mice, in which Ror2 was successfully deleted in the Gli1+ cells (Figure 6B). Three weeks after tamoxifen induction, Gli1+ MSCs were reduced in the incisor mesenchyme of *Gli1-CreER^{T2};Ror2$^{fl/fl}$;Gli1-LacZ* mice, indicating that Ror2-mediated non-canonical WNT signaling is critical for the maintenance of Gli1+ MSCs (Figures 6C-6G). The reduction of MSCs was further confirmed by LRCs (Figure 6-figure supplement 1). Taken together, our data indicate that non-canonical WNT signaling mediated by Wnt5a and Ror2 is involved in the TAC feedback to MSCs in regulating tissue homeostasis.

Discussion

The homeostatic maintenance of self-renewing tissue relies not only on the function of resident somatic stem and progenitor cells, but also on the interaction between these cell populations. In the present work, we studied the adult mouse incisor to uncover novel insights into the interaction between MSCs and TACs (Figure 7). Our data demonstrate that the IGF-WNT signaling cascade is crucial for MSC feedforward to TACs. In parallel, TACs feedback to MSCs via Wnt5a/Ror2-mediated non-canonical WNT signaling. Distinct genetic programs within TACs and MSCs may determine their *in vivo* identities and facilitate this dynamic reciprocal interaction to maintain mesenchymal tissue homeostasis.

Molecular signaling between stem cells and TACs

The question of which genetic programs determine the identities of stem cells and their progeny remains open. Previous studies have addressed this issue in epithelial stem cells. Hsu and colleagues found that TAC-derived SHH is critical in the hair follicle epithelium for stem cell activation and proliferation[19]. Another recent study defined gene signatures specific to stem cells and TACs in the hair follicle using RNA sequencing and subsequent transcriptomic analysis[6]. Single-cell RNA sequencing and lineage-tracing studies have revealed that hair follicle TACs represent a heterogeneous population of progenitors with distinct molecular signatures, reflecting different local signals and intercellular interactions according to their spatial locations[20]. Hair follicle TACs appear to be lineage-biased, as different cells preferentially give rise to seven cell types. In the dental epithelium, Hippo pathway components Yap and Taz are expressed in TACs and prevent their premature differentiation; Yap/Taz activate mTOR signaling to promote TAC proliferation in response to integrin/FAK signaling[21].

Despite this evolving understanding of epithelial stem cells and TACs, the distinct genetic signatures distinguishing MSCs from TACs are largely unknown. In our study, we identified genes that are differentially expressed in MSCs and TACs through RNA sequencing analysis. We found that several pathways related to cell proliferation, such as the mTOR signaling, were highly enriched in TACs[22,23], consistent with their high proliferative activity. On the other hand, growth factor signaling pathways were enriched in MSCs, including IGF, which has been previously implicated in stem cell homeostasis[14,15,24], suggesting that MSCs may secrete these factors to orchestrate their niche environment. Finally, these different signaling pathways may work together to build the identities of MSCs and TACs and facilitate the interaction between them to maintain tissue homeostasis. This model may serve as a stepping stone in our quest to gain a better understanding of MSCs and their interaction with neighboring cells in regulating tissue homeostasis.

Stem cell-TAC interaction in tissue homeostasis and regeneration

TACs are important progenitors that represent an intermediate step between MSCs and their differentiated progeny. Several recent findings have indicated that TACs are crucial to tissue regeneration. Specifically, TACs coordinate tissue production, govern stem cell behaviors, and instruct niche remodeling[25,26,27]. Recent studies also suggest that TACs may maintain homeostasis long-term in some cases, and thus may not actually be transient in nature[28,29]. These findings highlight several previously unrecognized functions of TACs, as well as the need to reevaluate their role in different biological states including homeostasis, regeneration, injury repair, and disease.

Recently, it has been suggested that some differentiated progeny of stem cells may serve as niche components and that interaction between stem cells and their progeny is critical for tissue homeostasis and regeneration. In the airway epithelium, stem/progenitor cells pass on a signal to their progeny that is necessary for daughter cell maintenance[9]. Moreover, some differentiated progeny of stem cells can also provide feedback to regulate their stem cell parents. In the intestine, terminally differentiated Paneth cells localized between crypt stem cells promote stem cell self-renewal[30]. Megakaryocytes regulate hematopoietic stem cell maintenance by regulating quiescence[31]. The progeny of stem cells might also be able to replenish them to maintain tissue homeostasis. For example, differentiated airway epithelial progenitor cells have been shown to revert into stem cells *in vivo* after the airway stem cells are ablated[32]. However, these studies have investigated only epithelial tissues and there is a lack of information about whether mesenchymal cells may participate in similar processes. In this study, we found that TACs in the mesenchyme have a profound impact on MSCs *in vivo* and that MSCs in turn instruct TACs via feedforward signals, indicating the existence of common regulatory mechanisms in the MSC niche environment.

Canonical and non-canonical WNT signaling work together to maintain MSCs and control TAC fate

Non-canonical WNT pathways are not well understood compared to their canonical counterpart, and most findings center around their ability to disrupt canonical WNT/β-catenin signaling[33]. During molar tooth development, Wnt5a plays a key role in regulating growth, patterning and development[18]. Previous study has also shown that non-canonical WNT signaling is required to maintain adult stem cells, including hematopoietic stem cells[34], and to mediate cell-cell interactions in some organs. Non-canonical WNT signaling might also regulate the interaction between MSCs and hematopoietic stem cells[35]. Wnt5a-Ror2 signaling between cells in the

283 osteoblast lineage and precursors of osteoclasts has been shown to enhance osteoclastogenesis and
284 maintain homeostasis during adult bone remodeling[36]. Depending on the receptor context, Wnt5a
285 can either activate or inhibit β-catenin signaling[37,38]. Cdc42-mediated non-canonical WNT
286 signaling has been shown to regulate neural stem cell quiescence in homeostasis and after
287 demyelination[39]. NFATc1 is involved in the balance of quiescence and proliferation in skin stem
288 cells[40,41], whereas NFATc4 regulates neural stem cells[42].

289 Here we report that Wnt5a acts through Ror2 to facilitate the feedback from TACs to MSCs in the
290 incisor mesenchyme, indicating a role for non-canonical WNT signaling in MSCs. TACs also
291 show strong canonical WNT signaling activity. The differential expression of WNT
292 receptors/intracellular mediators in the adult incisor mesenchyme may determine whether
293 canonical or non-canonical WNT signaling is activated, thereby affecting the crosstalk between
294 TACs and MSCs that controls mesenchymal tissue homeostasis. These two signaling pathways
295 work in concert to keep different cell types in proper balance and help MSCs and TACs coordinate
296 the homeostatic demands of the mouse incisor.

297 In conclusion, we have identified reciprocal interaction between MSCs and TACs using the adult
298 mouse incisor as a model. Our findings illustrate how MSCs feedforward to TACs, and how in
299 turn TACs produce crucial signals that sustain MSCs. Collectively, our results demonstrate that
300 the maintenance of adult tissue homeostasis requires not only stem cells and progenitor cells such
301 as TACs, but also reciprocal cell-cell interactions between them. It is reasonable to view the stem
302 cell niche as a local ecosystem that helps to maintain proper stem cell activity by promoting
303 crosstalk between stem cells and their progeny, which together preserve tissue homeostasis.

Materials and Methods

Key resource table

Reagent type (species) or resource	Designation	Source or reference	Identifiers	Additional information
strain, strain background (M. musculus)	*Axin2-CreER^{T2}*	Jackson Laboratory	Stock No. 018867 RRID:IMSR_JAX: 018867	
strain, strain background (M. musculus)	*Dmp1-Cre*	Jackson Laboratory	Stock No. 023047 RRID:IMSR_JAX: 023047	
strain, strain background (M. musculus)	*Gli1-CreER^{T2}*	Jackson Laboratory	Stock No. 007913 RRID:IMSR_JAX: 007913	
strain, strain background (M. musculus)	*Gli1-LacZ*	Jackson Laboratory	Stock No. 008211 RRID:IMSR_JAX: 008211	
strain, strain background (M. musculus)	*Igf1r$^{fl/fl}$*	Jackson Laboratory	Stock No. 012251 RRID:IMSR_JAX: 012251	
strain, strain background (M. musculus)	*Ror2$^{flox/flox}$*	Jackson Laboratory	Stock No. 018354 RRID:IMSR_JAX: 018354	
strain, strain background (M. musculus)	*Rosa26$^{<fs\text{-}tdTomato>}$*	Jackson Laboratory	Stock No. 007905 RRID:IMSR_JAX: 007905	
strain, strain background (M. musculus)	*Wnt5a$^{flox/flox}$*	Jackson Laboratory	Stock No. 026626 RRID:IMSR_JAX: 026626	
strain, strain background (M. musculus)	*Wls$^{flox/flox}$*	Jackson Laboratory	Stock No. 012888 RRID:IMSR_JAX: 012888	
genetic reagent (M. musculus)	anti-Axin2 probe	Advanced Cell Diagnostics	Cat# 400331	

genetic reagent (M. musculus)	anti-Fgf10 probe	Advanced Cell Diagnostics	Cat#446371	
genetic reagent (M. musculus)	anti-Fzd2 probe	Advanced Cell Diagnostics	Cat#404881	
genetic reagent (M. musculus)	anti-Fzd4 probe	Advanced Cell Diagnostics	Cat#404901	
genetic reagent (M. musculus)	anti-Fzd6 probe	Advanced Cell Diagnostics	Cat#404921	
genetic reagent (M. musculus)	anti-Igf1r probe	Advanced Cell Diagnostics	Cat#417561	
genetic reagent (M. musculus)	anti-Igf2 probe	Advanced Cell Diagnostics	Cat#437671	
genetic reagent (M. musculus)	anti-Igfbp3 probe	Advanced Cell Diagnostics	Cat#405941	
genetic reagent (M. musculus)	anti-Lrp5 probe	Advanced Cell Diagnostics	Cat#315791	
genetic reagent (M. musculus)	anti-Ror2 probe	Advanced Cell Diagnostics	Cat#430041	
genetic reagent (M. musculus)	anti-Wnt1 probe	Advanced Cell Diagnostics	Cat#401091	
genetic reagent (M. musculus)	anti-Wnt2 probe	Advanced Cell Diagnostics	Cat#313601	
genetic reagent (M. musculus)	anti-Wnt2b probe	Advanced Cell Diagnostics	Cat#405031	

genetic reagent (M. musculus)	anti-Wnt3 probe	Advanced Cell Diagnostics	Cat#312241	
genetic reagent (M. musculus)	anti-Wnt3a probe	Advanced Cell Diagnostics	Cat#405041	
genetic reagent (M. musculus)	anti-Wnt4 probe	Advanced Cell Diagnostics	Cat#401101	
genetic reagent (M. musculus)	anti-Wnt5a probe	Advanced Cell Diagnostics	Cat#316791	
genetic reagent (M. musculus)	anti-Wnt5b probe	Advanced Cell Diagnostics	Cat#405051	
genetic reagent (M. musculus)	anti-Wnt6 probe	Advanced Cell Diagnostics	Cat#401111	
genetic reagent (M. musculus)	anti-Wnt7a probe	Advanced Cell Diagnostics	Cat#401121	
genetic reagent (M. musculus)	anti-Wnt7b probe	Advanced Cell Diagnostics	Cat#401131	
genetic reagent (M. musculus)	anti-Wnt8a probe	Advanced Cell Diagnostics	Cat#405061	
genetic reagent (M. musculus)	anti-Wnt8b probe	Advanced Cell Diagnostics	Cat#405071	
genetic reagent (M. musculus)	anti-Wnt9a probe	Advanced Cell Diagnostics	Cat#405081	
genetic reagent (M. musculus)	anti-Wnt9b probe	Advanced Cell Diagnostics	Cat#405091	

genetic reagent (M. musculus)	anti-Wnt10a probe	Advanced Cell Diagnostics	Cat#401061	
genetic reagent (M. musculus)	anti-Wnt10b probe	Advanced Cell Diagnostics	Cat#401071	
genetic reagent (M. musculus)	anti-Wnt11 probe	Advanced Cell Diagnostics	Cat#405021	
genetic reagent (M. musculus)	anti-Wnt16 probe	Advanced Cell Diagnostics	Cat#401081	
antibody	anti-β-actin (Rabbit monoclonal)	Cell Signaling Technology	Cat#4970S RRID:AB_2223172	(1:2000)
antibody	Anti-Amelx (Rabbit polyclonal)	Abcam	Cat# ab153915	(1:100)
antibody	anti-β-catenin (Rabbit monoclonal)	Cell Signaling Technology	Cat#8814S RRID:AB_11127203	IF (1:100), WB (1:2000)
antibody	anti-β-gal (Chicken polyclonal)	Abcam	Cat#ab9361 RRID:AB_307210	(1:100)
antibody	anti-c-Myc (Rabbit monoclonal)	Abcam	Cat#ab32072 RRID:AB_731658	(1:100)
antibody	anti-Ki67 (Rabbit monoclonal)	Abcam	Cat# ab16667; RRID:AB_302459	(1:200)
antibody	anti-Wls (Chicken polyclonal)	Abcam	Cat#ab72385 RRID:AB_1269023	(1:200)

antibody	anti-Chicken (Goat polyclonal)	Life Technologies	Cat#A-11039 RRID:AB_142924	(1:200)
antibody	anti-Rabbit (Goat polyclonal)	Life Technologies	Cat#A-11011 RRID:AB_143157	(1:200)
antibody	anti-Chicken (Goat polyclonal)	Life Technologies	Cat#A-11041 RRID:AB_2534098	(1:200)
commercial assay or kit	RNeasy Micro Kit	QIAGEN	Cat# 74004	
commercial assay or kit	Click-iT™ EdU Cell Proliferation Kit	Thermo Fisher Scientific	Cat# C10337	
software, algorithm	ImageJ	NIH	RRID:SCR_003070	
software, algorithm	GraphPad Prism	GraphPad Software	RRID:SCR_002798	

Animals and Procedures

Axin2-CreER^{T2}, *Dmp1-Cre*, *Gli1–CreER^{T2}*, *Gli1–LacZ*, *Igf1r$^{flox/flox}$*, *Ror2$^{flox/flox}$*, *Rosa26$^{<fs\text{-}tdTomato>}$*, *Wnt5a$^{flox/flox}$* and *Wls $^{flox/flox}$* mouse strains were cross-bred as needed for this study. All mouse experiments were conducted in accordance with protocol 20299 approved by the Department of Animal Resources and the Institutional Animal Care and Use Committee of the University of Southern California.

Mice were housed in pathogen-free conditions, identified via ear tags, and analyzed in a mixed background. Tail biopsies were lysed through incubation at 55°C overnight in DirectPCR tail solution (Viagen 102-T) followed by 30 minutes of heat inactivation at 85°C prior to PCR-based

genotyping (GoTaq Green MasterMix, Promega, and C1000 Touch Cycler, Bio-rad). Mice were euthanized by carbon dioxide overdose followed by cervical dislocation. All mice were used for analysis regardless of sex.

For $CreER^{T2}$ activation, tamoxifen (Sigma) was dissolved in corn oil (20 mg/ml) and injected intraperitoneally.

Immunofluorescence and in situ hybridization (ISH)

Mouse mandibles were dissected, fixed in 4% PFA overnight, and decalcified with 10% EDTA for four weeks. The tissues were next incubated with 15% sucrose for two hours and 30% sucrose overnight, then embedded in OCT. Frozen tissue blocks were sectioned at 10 mm on a cryostat (Leica) and mounted on SuperFrost Plus slides (Fisher). The tissue sections were blocked for one hour at room temperature in blocking solution (Vector Laboratories). Sections were then incubated with primary antibodies diluted in blocking solution at 4°C overnight. After three washes with PBS, sections were incubated with secondary antibodies in blocking solution at room temperature for one hour. DAPI was used to stain nuclei and all images were acquired using a Keyence microscope (Carl Zeiss). Non-immune immunoglobulins of the same isotype as the primary antibodies were used as negative controls.

In situ hybridization (ISH) was performed using an RNAscope 2.5 HD Chromogenic Assay (Single-plex, Advanced Cell Diagnostics). Briefly, tissues were fixed in 4% PFA overnight at room temperature before cryosectioning into 10 μm sections, after which ISH was performed according to the manufacturer's instructions.

MicroCT analysis

MicroCT analysis was performed using a SCANCO μCT50 device at the University of Southern California Molecular Imaging Center. Images were acquired with the x-ray source at 70 kVp and 114 μA. Images were generated at a resolution of 10 μm. Three-dimensional reconstruction was achieved using AVIZO 7.1 (Visualization Sciences Group).

Laser capture microdissection (LCM)

We euthanized one-month-old *Axin2-CreER^{T2};Rosa26$^{<fs\text{-}tdTomato>}$* and *Gli1-CreER^{T2};Rosa26$^{<fs\text{-}tdTomato>}$* (n=3 per group) one day after the injection of tamoxifen. After quickly dissecting out the mandible and rinsing in PBS and OCT, the samples were transferred into a mold filled with pre-cooled OCT and frozen using liquid nitrogen. Next, the samples were sectioned to 10 μm thickness and mounted on Polyethylenenaphthalate (PEN)-membrane slides (Zeiss). After UV treatment for 30 minutes, we performed LCM of the Axin2+ and Gli1+ cells using the Zeiss PALM Laser Capture Microdissection System.

RNA sequencing

Incisor samples from LCM of one-month-old *Axin2-CreER^{T2};Rosa26$^{<fs\text{-}tdTomato>}$* and *Gli1-CreER^{T2};Rosa26$^{<fs\text{-}tdTomato>}$* mice were collected for RNA isolation using an RNeasy Micro Kit (QIAGEN). The quality of RNA samples was determined using an Agilent 2100 Bioanalyzer and only those with RNA integrity (RIN) numbers > 7.0 were used for sequencing. cDNA library preparation and sequencing were performed at the Epigenome Center of the University of Southern California. Single-end reads with 75 cycles were performed on an Illumina Hiseq 4000 for three pairs of samples. Raw reads were trimmed, aligned with the mm10 genome using TopHat (version 2.0.8), and normalized using RPKM. Differential expression was calculated by selecting transcripts with a significance level set to $P < 0.05$.

Immunoblotting

For immunoblotting, mouse incisor mesenchyme was lysed in lysis buffer (50 mM Tris-HCl pH 7.5, 150 mM NaCl, 2mM EDTA, 0.1% NP-40, 10% glycerol, and protease inhibitor cocktail). Proteins were quantified using Bio-Rad protein assay (Bio-Rad Laboratories), and 20-80 μg of protein was separated by SDS-PAGE and transferred to 0.45 μm PVDF membrane. Membranes were blocked in TBST and 5% BSA (blocking solution) for 1 h, followed by overnight incubation with active β-catenin antibody diluted at 1:2000 in blocking solution, and 1 h incubation with HRP-conjugated secondary antibody diluted at 1:2000. Immunoreactive protein was detected using ECL (GE Healthcare) and film.

Label-retaining cell analysis

Mice were given i.p. injections of EdU (150 mg/kg) daily for two weeks. Samples were collected one month after the last injection and processed for further analysis with the Click-iT™ EdU Cell Proliferation Kit based on the manufacturer's protocol.

Statistical analysis

Prism 7 (GraphPad) was used for statistical analysis. All bar graphs display mean ± SD (standard deviation). Significance was assessed by independent two-tailed Student's t tests or ANOVA. $p < 0.05$ was considered statistically significant.

ImageJ image analysis

ImageJ was used to determine the percentage of immunostained area. Images of the TAC and MSC regions were first converted to 8-bit binary and evaluated for positive immunofluorescence signal using the ''Analyze Particles'' function. The derived area was then divided by the total area of TAC or MSC regions to calculate the percentage of positive immunostaining.

Data availability

The GEO accession number for the RNA sequencing data reported in this paper is GSE109876.

Acknowledgements

We thank Julie Mayo and Bridget Samuels for critical reading of the manuscript. We acknowledge USC Libraries Bioinformatics Service for assisting with data analysis. The bioinformatics software and computing resources used in the analysis are funded by the USC Office of Research and the Norris Medical Library. This study was supported by grants from the National Institute of Dental and Craniofacial Research, National Institutes of Health (R01 DE025221 and R01 DE012711).

Competing interests

The authors declare no competing interests.

Author information

Correspondence and requests for materials should be addressed to Y.C. (ychai@usc.edu).

References

1. Barker N, van Oudenaarden A, Clevers H. Identifying the stem cell of the intestinal crypt:strategies and pitfalls. Cell Stem Cell 11, 452-460 (2012).
2. Jensen KB, Watt FM. Single cell expression profiling of human epidermal stem and transit-amplifying cells: Lrig1 is a regulator of stem cell quiescence. Proc Natl Acad Sci U S A. 103, 11958-11963 (2006).
3. Lui JH, Hansen DV, Kriegstein AR. Development and evolution of the human neocortex. Cell. 146, 18-36 (2011).
4. Scadden DT. Nice neighborhood: Emerging concepts of the stem cell niche. Cell 157, 41-50 (2014).
5. Xin T, Greco V, Myung P. Hardwiring stem cell communication through tissue structure. Cell 164, 1212-1225 (2016).
6. Rezza A, et al. Signaling networks among stem cell precursors, transit-amplifying progenitors, and their niche in developing hair follicles. Cell Rep. 14, 3001-3018 (2016).
7. Hsu YC, Fuchs E. A family business: stem cell progeny join the niche to regulate homeostasis. Nat. Rev. Mol. Cell Biol. 13, 103-114 (2012).
8. Hsu YC, Li L, Fuchs E. Transit-amplifying cells orchestrate stem cell activity and tissue regeneration. Cell 157, 935-949 (2014).
9. Pardo-Saganta A, et al. Parent stem cells can serve as niches for their daughter cells. Nature 523, 597-601 (2015).
10. An Z, et al. Regulation of mesenchymal stem to transit-amplifying cell transition in the continuously growing mouse incisor. Cell Rep. 23(10):3102-3111 (2018).
11. Sharpe PT. Dental mesenchymal stem cells. Development. 143, 2273-2280 (2016).

12. Zhao H, et al. Secretion of Shh by a neurovascular bundle niche supports mesenchymal stem cell homeostasis in the adult mouse incisor. Cell Stem Cell 14, 160-173 (2014).
13. Kaukua N, et al. Glial origin of mesenchymal stem cells in a tooth model system. Nature 513, 551-554 (2014).
14. Youssef A, Aboalola D, Han VK. The roles of insulin-like growth factors in mesenchymal stem cell niche. Stem Cells Int. 2017, 9453108 (2017).
15. Ziegler AN, Levison SW, Wood TL. Insulin and IGF receptor signaling in neural-stem-cell homeostasis. Nat Rev Endocrinol. 11, 161-170 (2015).
16. Kuang-Hsien Hu J, Mushegyan V, Klein OD. On the cutting edge of organ renewal: Identification, regulation, and evolution of incisor stem cells. Genesis 52, 79-92 (2014).
17. Wang XP, et al. An integrated gene regulatory network controls stem cell proliferation in teeth. PLoS Biol. 5, e159 (2007).
18. Lin M, et al. Wnt5a regulates growth, patterning, and odontoblast differentiation of developing mouse tooth. Dev Dyn. 240, 432-440 (2011).
19. Hsu YC, Li L, Fuchs E. Emerging interactions between skin stem cells and their niches. Nat. Med. 20, 847-56 (2014).
20. Yang H, Adam RC, Ge Y, Hua ZL, Fuchs E. Epithelial-mesenchymal micro-niches govern stem cell lineage choices. Cell 169, 483-496 (2017).
21. Hu JK, et al. An FAK-YAP-mTOR signaling axis regulates stem cell-based tissue renewal in mice. Cell Stem Cell 21, 91-106 (2017).
22. Laplante M, Sabatini DM. mTOR signaling in growth control and disease. Cell 149, 274-293 (2012).

437 23. Saxton RA, Sabatini DM. mTOR signaling in growth, metabolism, and disease. Cell 169, 361-
438 371 (2017).
439 24. Xian L, et al. Matrix IGF 1 maintains bone mass by activation of mTOR in mesenchymal stem
440 cells. Nat. Med. 18, 1095-1101 (2012).
441 25. Zhang B, et al. Hair follicles' transit-amplifying cells govern concurrent dermal adipocyte
442 production through Sonic Hedgehog. Genes Dev. 30, 2325-2338 (2016).
443 26. Zhang B, Hsu YC. Emerging roles of transit-amplifying cells in tissue regeneration and cancer.
444 Wiley Interdiscip Rev Dev Biol 6, 1-14 (2017).
445 27. Carrieri C, et al. A transit-amplifying population underpins the efficient regenerative capacity
446 of the testis. J Exp Med. 214, 1631-1641 (2017).
447 28. Busch K, Klapproth K, Barile M. Fundamental properties of unperturbed haematopoiesis from
448 stem cells in vivo. Nature 518, 542-546 (2015).
449 29. Sun J, et al. Clonal dynamics of native haematopoiesis. Nature 514, 322-327 (2014).
450 30. Sato T, et al. Paneth cells constitute the niche for Lgr5 stem cells in intestinal crypts. Nature
451 469, 415-418 (2011).
452 31. Bruns I, et al. Megakaryocytes regulate hematopoietic stem cell quiescence through CXCL4
453 secretion. Nat. Med. 20, 1315-1320 (2014).
454 32. Tata PR, et al. Dedifferentiation of committed epithelial cells into stem cells in vivo. Nature
455 503, 218-223 (2013).
456 33. Lien WH, Fuchs E. Wnt some lose some: transcriptional governance of stem cells by Wnt/β-
457 catenin signaling. Genes Dev. 28, 1517-1532 (2014).
458 34. Sugimura R, et al. Noncanonical Wnt signaling maintains hematopoietic stem cells in the niche.
459 Cell 150, 351-365 (2012).

460 35. Sugimura R, Li L. Noncanonical Wnt signaling in vertebrate development, stem cells, and
461 diseases. Birth Defects Res C Embryo Today. 90, 243-256 (2010).
462 36. Maeda K, et al. Wnt5a-Ror2 signaling between osteoblast-lineage cells and osteoclast
463 precursors enhances osteoclastogenesis. Nat. Med. 18, 405-412 (2012).
464 37. Mikels AJ, Nusse R. Purified Wnt5a protein activates or inhibits beta-catenin-TCF signaling
465 depending on receptor context. Plos Biol. 4, e115 (2006).
466 38. Van Amerongen R, Bowman AN, Nusse R. Developmental stage and time dictate the fate of
467 Wnt/β-catenin-responsive stem cells in the mammary gland. Cell Stem Cell 11, 387-400 (2012).
468 39. Chavali M, et al. Non canonical Wnt signaling regulates neural stem cell quiescence during
469 homeostasis and after demyelination. Nat Commun. 9, 36 (2018).
470 40. Goldstein J, et al. Calcineurin/Nfatc1 signaling links skin stem cell quiescence to hormonal
471 signaling during pregnancy and lactation. Genes Dev. 28, 983-994 (2014).
472 41. Horsley V, Aliprantis AO, Polak L, Glimcher LH, Fuchs E. NFATc1 balances quiescence and
473 proliferation of skin stem cells. Cell 132, 299-310 (2008).
474 42. Moreno M, et al. Transcriptional profiling of hypoxic neural stem cells identifies calcineurin-
475 NFATc4 signaling as a major regulator of neural stem cell biology. Stem Cell Reports 5, 157-
476 165 (2015).

Figure Legends

Figure 1. *In vivo* anatomical and molecular identities of MSCs and TACs in the mouse incisor. (A-B) Ki67 staining (green), tdTomato visualization (red), and DAPI staining (blue) of incisors from one-month-old *Axin2-CreER^{T2};Rosa26$^{<fs\text{-}tdTomato>}$* mice one day after tamoxifen (TM) induction. (C-D) β-gal staining (green) and Ki67 immunofluorescence (red) of incisors from one-month-old *Gli1-LacZ* mice. Box in (C) is shown enlarged in (D). (E) Schematic diagram of MSCs and TACs in the mouse incisor. Arrows indicate positive signal. Schematics at the bottom indicate induction protocols. The white dashed lines outline the cervical loop. Scale bars, 100μm.

Figure 2. IGF ligand and binding proteins are highly enriched in MSCs. (A) Top eight signaling pathways enriched in TACs identified by Ingenuity Pathway Analysis. (B) IGF signaling molecules enriched in MSCs. (C-H) RNAscope (red) of Igfbp3 (C-D), Igf2 (E-F) and Igf1r (G-H) in incisors of one-month-old control mice. Boxes in (C, E, and G) shown magnified in (D, F, and H), respectively. Arrows indicate positive signal. The white dashed lines outline the cervical loop. Scale bars, 100 μm.

Figure 3. Inactivation of IGF signaling leads to TAC loss in the incisor mesenchyme. (A-D) H&E staining and Ki67 immunofluorescence (red) of incisors from *Igf1r$^{fl/fl}$* (control) and *Axin2-CreER^{T2};Igf1r$^{fl/fl}$* mice. Black arrow in (A) indicates normal dentin and black arrow in (B) indicates thicker dentin. White arrow in (C) indicates a positive signal and asterisk in (D) indicates diminished signal. (E) Quantitation of the percentage of Ki67+ TACs from (C-D). (F-G) Immunostaining of Axin2 expression (red) in incisors from *Igf1r$^{fl/fl}$* (control) and *Axin2-CreER^{T2};Igf1r$^{fl/fl}$* mice. White arrow in (F) indicates a positive signal and asterisk in (G) indicates absence of a signal. (H) Diagram depicts our model of the Igf2-WNT signaling cascade. Quantitative data are presented as mean± SD. ****, $p<0.0001$. Schematics at the bottom indicate

induction protocols. The white dashed lines outline the cervical loop. Four mice with four sections within each mouse per group were used to quantify Ki67 + cells. Scale bars, 100 μm.

Figure 3-Source data 1. Source data for Figure 3E.

Figure 3-figure supplement 1. Effect of the incisor mesenchyme is primary in TAC loss in *Axin2-CreER^{T2};Igf1r$^{fl/fl}$* incisors. (A-B) Ki67 immunostaining of *Igf1r$^{fl/fl}$* and *Axin2-CreER^{T2};Igf1r$^{fl/fl}$* incisors one week after tamoxifen induction. (C-D) Quantitative analysis of Ki67+ TACs in the mesenchyme and epithelium of *Igf1r$^{fl/fl}$* and *Axin2-CreER^{T2};Igf1r$^{fl/fl}$* incisors one week after tamoxifen induction. (E-H) RNAscope staining of *Dspp* and immunostaining of Amelx in *Igf1r$^{fl/fl}$* and *Axin2-CreER^{T2};Igf1r$^{fl/fl}$* incisors one week after tamoxifen induction. Quantitative data are presented as mean± SD. *, $p<0.05$. ns, no significance. Schematics at the bottom indicate induction protocols. White arrows in E and G indicate the position where odontoblasts start. The white dashed lines outline the cervical loop. Four mice per group, with four sections per mouse, were used to quantify Ki67 + cells. Scale bars, 100 μm.

Figure 3-figure supplement 1-Source data 1. Source data for Figure 3-figure supplement 1C and 1D.

Figure 3-figure supplement 2. Canonical WNT signaling is downregulated after loss of Igf1r in the TACs of the mouse incisor. (A-D) Immunostaining of c-Myc and active β-catenin in incisors from *Igf1r$^{fl/fl}$* (control) and *Axin2-CreER^{T2};Igf1r$^{fl/fl}$* mice. The white dashed lines outline the cervical loop. Arrows indicate positive signal and asterisks indicate diminished signal. Schematics at the bottom indicate induction protocols. Scale bars, 100 μm. (E) Western blot of active β-catenin in incisors from *Igf1r$^{fl/fl}$* and *Axin2-CreER^{T2};Igf1r$^{fl/fl}$* mice.

Figure 3-figure supplement 3. Long-term phenotype of *Axin2-CreER^{T2};Igf1r$^{fl/fl}$* incisors. (A-F) H&E and RNAscope staining of Dspp (red) and Ki67 staining (red) of incisors from *Igf1r$^{fl/fl}$* (control) and *Axin2-CreER^{T2};Igf1r$^{fl/fl}$* mice five months after tamoxifen induction. Black arrow in A indicates normal dentin and black arrow in D indicates thicker dentin. White arrows in B and E indicate the position where odontoblasts start. White arrow in C indicates positive signal and asterisk in F indicates diminished signal. White dashed lines outline the cervical loop. Schematics at the bottom indicate induction protocols. Scale bars, 100 μm.

Figure 4. Signaling enriched in MSCs and WNT ligand enriched in TACs. (A) Wnt10a and Wnt5a are enriched in TACs. (B-E) RNAscope (red) of Wnt10a and Wnt5a in incisors from one-month-old control mice. (F) Top eight signaling pathways enriched in MSCs identified by Ingenuity Pathway Analysis. Boxes in (B and D) are shown magnified in (C and E), respectively. Arrows indicate positive signal. The white dashed lines outline the cervical loop. The yellow dashed line outlines the MSC region. Scale bars, 100μm.

Figure 4-figure supplement 1. WNT ligand expression in adult incisors. (A-Q') RNAscope (red) of Wnt3a (A-A'), Wnt4 (B-B'), Wnt1 (C-C'), Wnt2 (D-D'), Wnt2b (E-E'), Wnt3 (F-F'), Wnt5b (G-G'), Wnt6 (H-H'), Wnt7a (I-I'), Wnt7b (J-J'), Wnt8a (K-K'), Wnt8b (L-L'), Wnt9a (M-M'), Wnt9b (N-N'), Wnt10b (O-O'), Wnt11 (P-P'), and Wnt16 (Q-Q') in incisors of one-month-old control mice. Boxes in (A-Q) are shown magnified in (A'-Q'), respectively. Insets in (A and B) show magnified images of the epithelium. The white dashed lines outline the cervical loop. Arrows indicate positive signal and asterisks indicate absence of signal. Scale bars, 100 μm.

Figure 4-figure supplement 2. Loss of WNT signaling in odontoblasts has no effect on MSCs or TACs. (A-D) H&E staining and Ki67 immunofluorescence (red) of incisors from two-month-old *Gli1-LacZ* (control) and *Dmp1-Cre;Wls$^{fl/fl}$;Gli1-LacZ* mice (mutant). (E) Quantitation of the

percentage of Ki67+ cells per higher magnification section (C, D) of *Gli1-LacZ* and *Dmp1-Cre;Wls$^{fl/fl}$;Gli1-LacZ* incisor mesenchyme. (F-I) β-gal staining (green) of incisors from two-month-old *Gli1-LacZ* and *Dmp1-Cre;Wls$^{fl/fl}$;Gli1-LacZ* mice. (J) Quantitation of the percentage of Gli1+ cells per higher magnification section (H, I) of *Gli1-LacZ* and *Dmp1-Cre; Wls$^{fl/fl}$;Gli1-LacZ* incisor mesenchyme. Arrows indicate positive signal. The white dashed lines outline the cervical loop. All quantitative data are presented as mean± SD. ns, no significance. Four mice with four sections within each mouse per group were used to quantify Ki67+ cells. Gli1+ cells in the proximal region between the two cervical loops were counted in the mouse incisor. Scale bars, 100 μm.

Figure 4-figure supplement 2-Source data 1. Source data for Figure 4-figure supplement 2E and 2J.

Figure 4-figure supplement 3. Loss of *Wls* in TACs results in diminished TACs and MSCs in the incisors of *Axin2-CreER^{T2};Wls$^{fl/fl}$;Gli1-LacZ* mice. (A-B) Wls immunofluorescence (red) and DAPI staining (blue) of incisors from two-month-old *Gli1-LacZ* (control) and *Axin2-CreER^{T2};Wls$^{fl/fl}$;Gli1-LacZ* mice. (C-D) MicroCT images of incisors from two-month-old *Gli1-LacZ* and *Axin2-CreER^{T2};Wls$^{fl/fl}$;Gli1-LacZ* mice induced with tamoxifen for one month. (E-H) Ki67 immunofluorescence (red) and RNAscope (red) of Fgf10 in incisors of two-month-old control and *Axin2-CreER^{T2};Wls$^{fl/fl}$;Gli1-LacZ* mice. (I-L) β-gal staining (green) of incisors from two-month-old *Gli1-LacZ* and *Axin2-CreER^{T2};Wls$^{fl/fl}$;Gli1-LacZ* mice. The white dashed lines outline the cervical loop. Arrow indicates positive signal and asterisk indicates absence of signal. Schematics at the bottom indicate induction protocols. Scale bars for (E-F), 2mm; Scale bars for others, 100 μm.

Figure 4-figure supplement 4. WNT receptor expression in adult incisors. (A-H) RNAscope (red) of Lrp5 (A-B), Fzd2 (C-D), Fzd4 (E-F), and Fzd6 (G-H) in incisors of one-month-old control mice. Boxes in (A, C, E, and G) are shown magnified in (B, D, F, and H), respectively. Arrows indicate positive signal and asterisks indicate absence of signal. Scale bars, 100 μm.

Figure 5. Loss of Wnt5a results in loss of Gli1+ MSCs. (A-B) Ki67 staining (red) of incisors from *Gli1-LacZ* (control) and *Axin2-CreER^{T2};Wnt5a$^{fl/fl}$;Gli1-LacZ* mice three weeks after tamoxifen induction. (C) Quantitation of the percentage of Ki67+ TACs from (A and B). (D-G) β-gal staining (green) of incisors from one-month-old *Gli1-LacZ* and *Axin2-CreER^{T2};Wnt5a$^{fl/fl}$;Gli1-LacZ* mice three weeks after tamoxifen induction. Boxes in (D and E) are shown magnified in (F and G), respectively. (H) Quantitation of the percentage of Gli1+ cells per higher magnification section (F, G) of *Gli1-LacZ* and *Axin2-CreER^{T2};Wnt5a$^{fl/fl}$;Gli1-LacZ* incisor mesenchyme. Schematics at the bottom indicate induction protocols. The white dashed lines outline the cervical loop. Arrows indicate positive signal and asterisks indicate diminished signal. All quantitative data are presented as mean± SD. ns, no significance. ****, $p<0.0001$. Four mice with four sections within each mouse per group were used to quantify Ki67+ cells. Gli1+ cells in the proximal region between the two cervical loops were counted in the mouse incisor. Scale bars, 100 μm.

Figure 5-Source data 1. Source data for Figure 5C and 5H.

Figure 5-figure supplement 1. Validation of *Wnt5a* knockout efficiency in *Axin2-CreER^{T2};Wnt5a$^{fl/fl}$* incisors. (A-D) RNAscope (red) of *Wnt5a* in incisors from *Wnt5a$^{fl/fl}$* (control) and *Axin2-CreER^{T2};Wnt5a$^{fl/fl}$* incisors three days after tamoxifen induction. White arrow indicates positive signal and asterisk indicates diminished signal. Schematics at the bottom indicate induction protocols. Scale bars, 100 μm.

Figure 5-figure supplement 2. Loss of Wnt5a results in diminished EdU+ LRCs. (A-D) EdU staining of *Wnt5a$^{fl/fl}$ and Axin2-CreER^{T2};Wnt5a$^{fl/fl}$* mouse incisors. (E) Quantification was performed by calculating the percentage of EdU+ cells per section under higher magnification (B, D) in *Wnt5a$^{fl/fl}$ and Axin2-CreER^{T2};Wnt5a$^{fl/fl}$* mouse incisor mesenchyme. Schematics underneath figures indicate induction protocols. All quantitative data are presented as mean ± SD. ***, $p<0.001$. Scale bars, 100 μm.

Figure 5-figure supplement 2-Source data 1. Source data for Figure 5-figure supplement 2E.

Figure 5-figure supplement 3. Loss of Wnt5a results in thicker dentin and diminished TACs. (A-D) H&E and Ki67 staining (red) of incisors from one-month-old *Wnt5a$^{fl/fl}$* (control) and *Axin2-CreER^{T2};Wnt5a$^{fl/fl}$* mice six weeks after tamoxifen induction. (E-H) H&E and Ki67 staining (red) of incisors from *Wnt5a$^{fl/fl}$* (control) and *Axin2-CreER^{T2};Wnt5a$^{fl/fl}$* mice five months after tamoxifen induction. Black arrows in A and E indicate normal dentin and black arrows in B and F indicates thicker dentin. White arrows in C and G indicate positive signal and asterisks in D and H indicate diminished signal. White dashed lines outline the cervical loop. Schematics at the bottom indicate induction protocols. Scale bars, 100 μm.

Figure 6. Ror2-mediated non-canonical Wnt signaling regulates MSC maintenance in the incisor. (A-B) RNAscope (red) of Ror2 in incisors from *Gli1-LacZ* (control) and *Gli1-CreER^{T2};Ror2$^{fl/fl}$;Gli1-LacZ* one-month-old mice. Insets in A and B show magnified images of the MSC region. (C-F) β-gal staining (green) of incisors from *Gli1-LacZ* and *Gli1-CreER^{T2};Ror2$^{fl/fl}$;Gli1-LacZ* mice. Boxes in C and D are shown magnified in E and F, respectively. (G) Quantification of the percentage of Gli1+ cells per higher magnification section of *Gli1-LacZ* (control) and *Gli1-CreER^{T2};Ror2$^{fl/fl}$;Gli1-LacZ* (mutant) mouse incisor mesenchyme in E and F. Gli1+ cells in the proximal region between the two cervical loops were counted in the mouse

incisor. Quantitative data are presented as mean± SD. ****, p<0.0001. Arrows indicate positive signal and asterisks indicate diminished signal. Schematics at the bottom indicate induction protocols. Scale bars, 100 μm.

Figure 6-Source data 1. Source data for Figure 6G.

Figure 6-figure supplement 1. Loss of Ror2 results in diminished EdU+ LRCs. (A-D) EdU staining of *Ror2$^{fl/fl}$ and Gli1-CreER^{T2};Ror2$^{fl/fl}$* mouse incisors. (E) Quantification was performed by calculating the percentage of EdU+ cells per section of *Ror2$^{fl/fl}$ and Gli1-CreER^{T2};Ror2$^{fl/fl}$* incisor mesenchyme under higher magnification (B, D). Schematics underneath figures indicate induction protocols. All quantitative data are presented as mean± SD. ****, p<0.0001. Scale bars, 100 μm.

Figure 6-figure supplement 1 Source data 1. Source data for Figure 6-figure supplement 1E.

Figure 7. Schematic diagram of bi-directional interaction between TACs and MSCs. Igf2 secreted from Gli1+ MSCs binds to Igf1r in the Axin2+ TACs, activating target gene expression and regulate TAC proliferation. Wnt5a serves as a non-canonical WNT ligand, feeding back to MSCs through Ror2 to activate downstream gene expression to regulate the maintenance of MSCs. Thus, MSCs and TACs dynamically interact with each other to maintain mesenchymal tissue homeostasis.

Figure 1

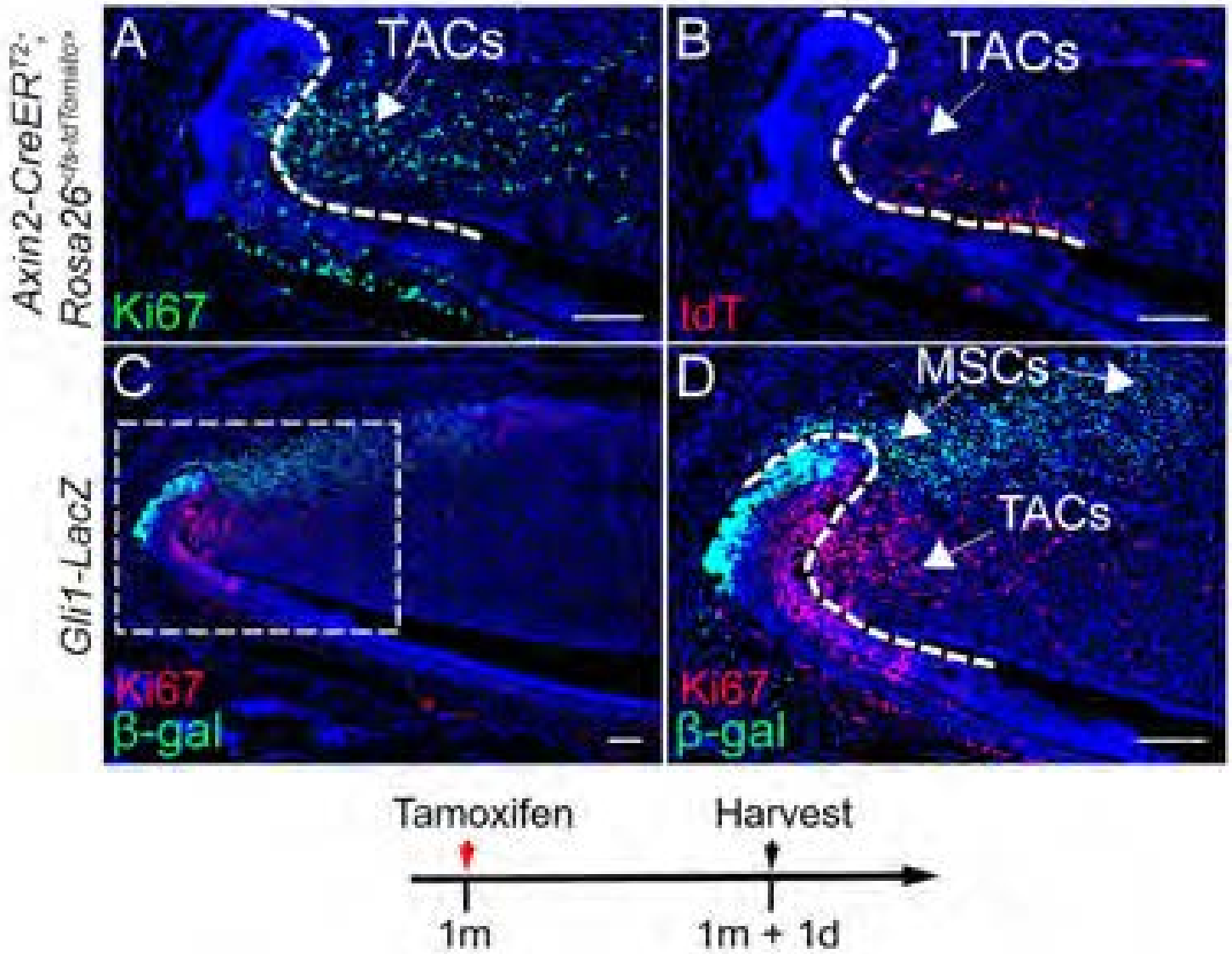
A
TACs
Ki67
B
TACs
IdT
Axin2-CreER^T2+
Rosa26^+/+tdTomato
C
Ki67
β-gal
Gli1-LacZ
D
MSCs
TACs
Ki67
β-gal
Tamoxifen
Harvest
1m
1m + 1d
E
Mesenchymal stem cells (MSCs—Gli1+)
Transit amplifying cells (TACs—Axin2+)
Gli1
Axin2

Figure 2

A

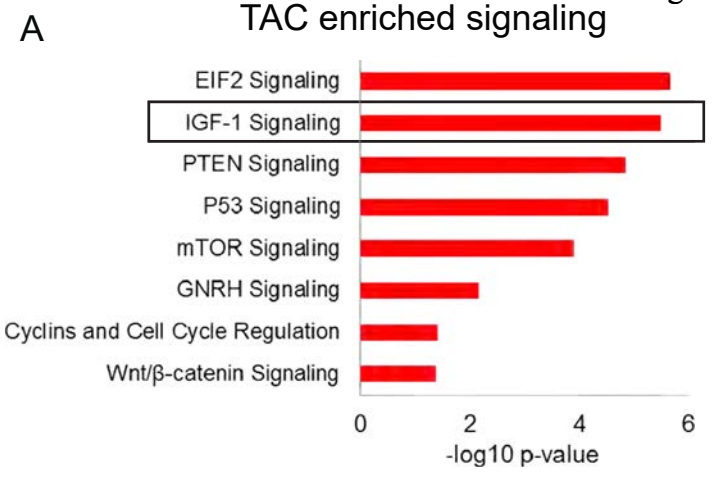

B

MSC enriched IGF signaling molecules

Genes	Fold change (MSC vs. TAC)
Igfbp3	68.86
Igf2	5.5

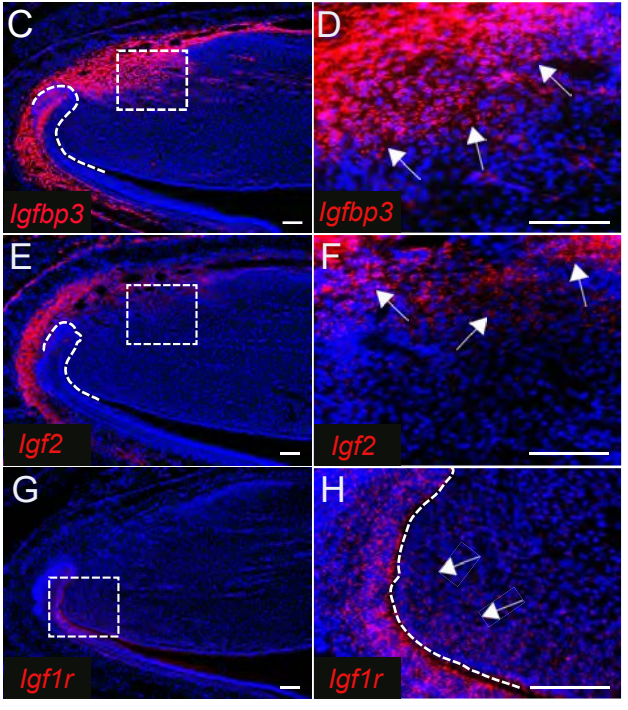

Figure 3

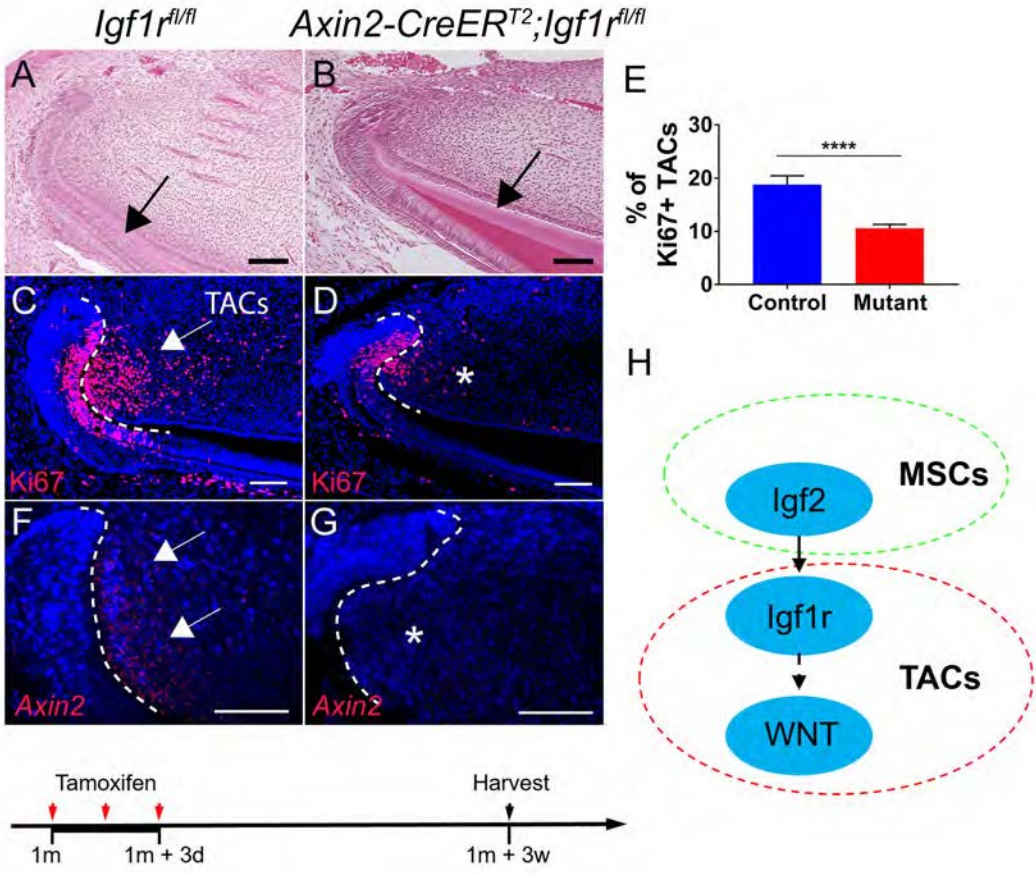
Igf1r^fl/fl
Axin2-CreER^T2;Igf1r^fl/fl
A
B
C
TACs
D
Ki67
Ki67
F
G
Axin2
Axin2
E
% of Ki67+ TACs
30
20
10
0
****
Control
Mutant
H
MSCs
Igf2
Igf1r
TACs
WNT
Tamoxifen
Harvest
1m
1m + 3d
1m + 3w

Figure 3-figure supplement 1

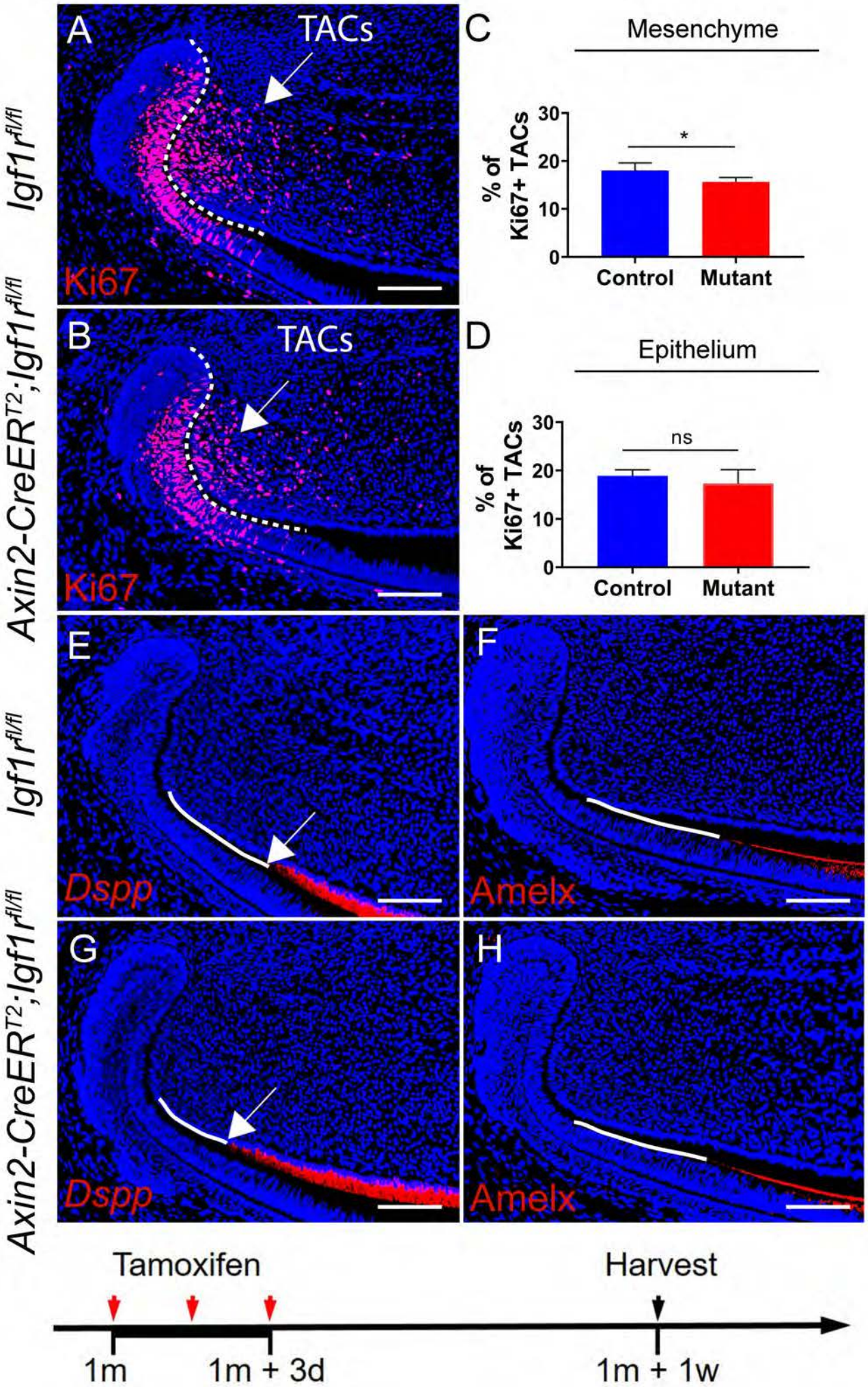

Figure 3-figure supplement 2

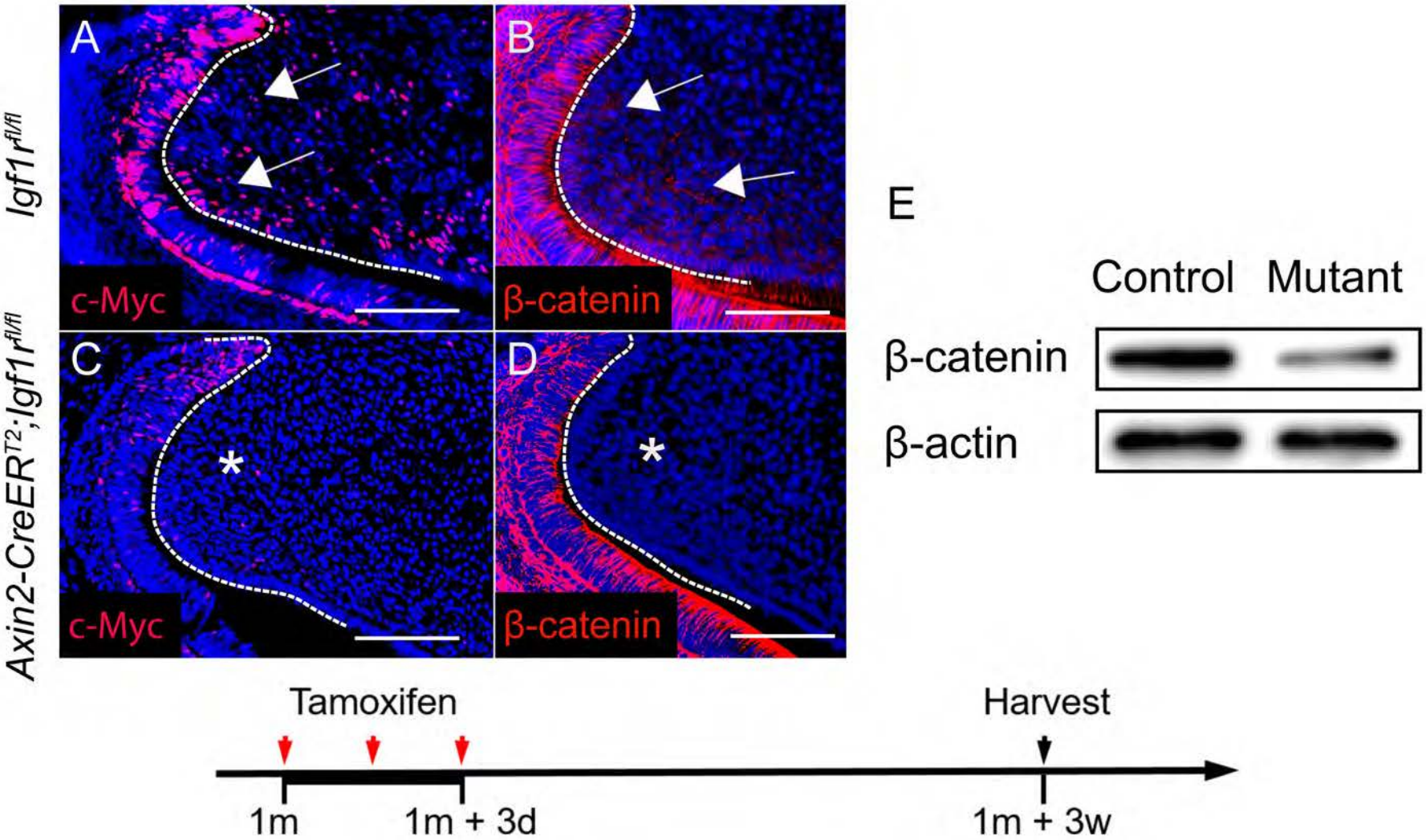

Figure 3-figure supplement 3

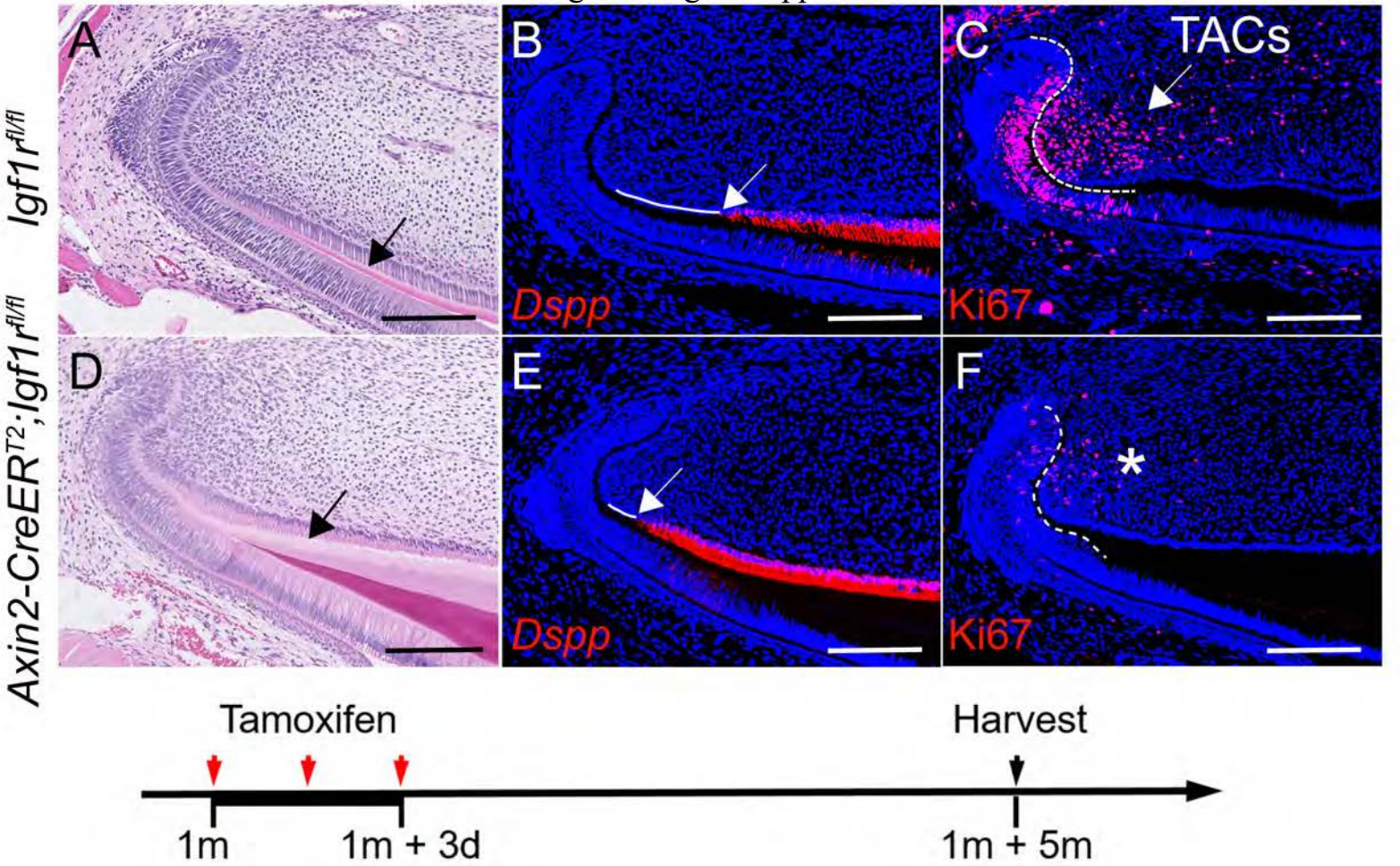

Figure 4

A

TAC enriched WNT ligand

Genes	Fold change (TAC vs. MSC)
Wnt5a	2.00
Wnt10a	3.53

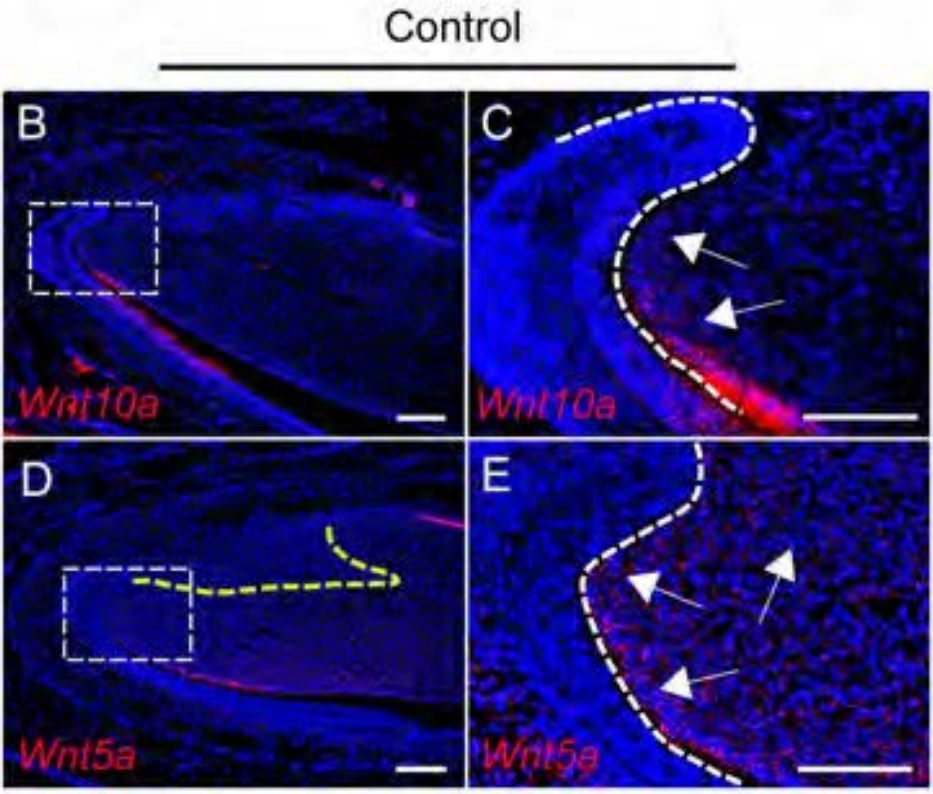

F

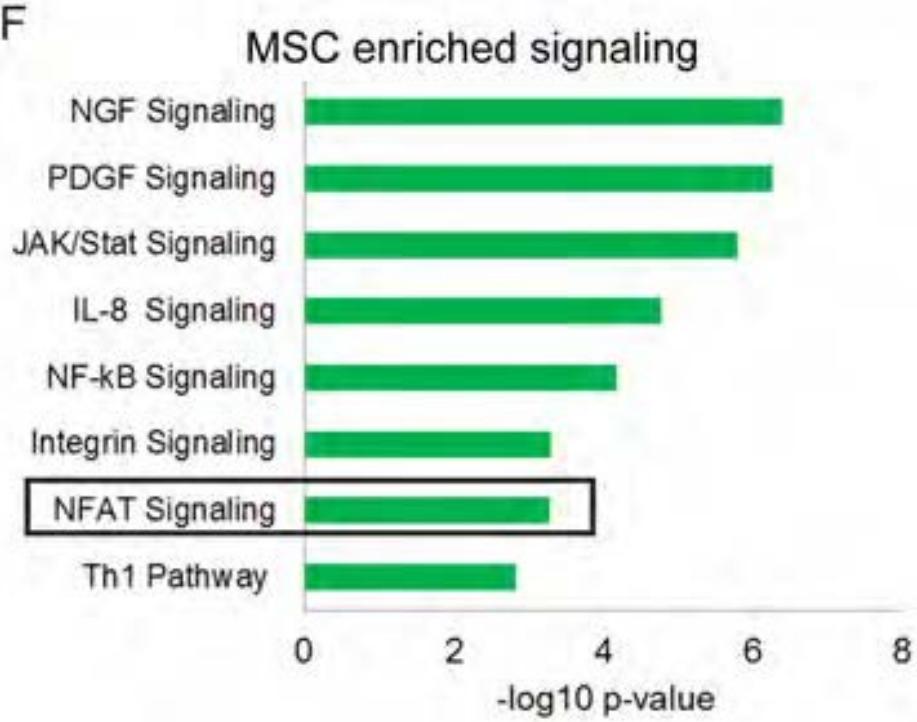

Figure 4-figure supplement 1

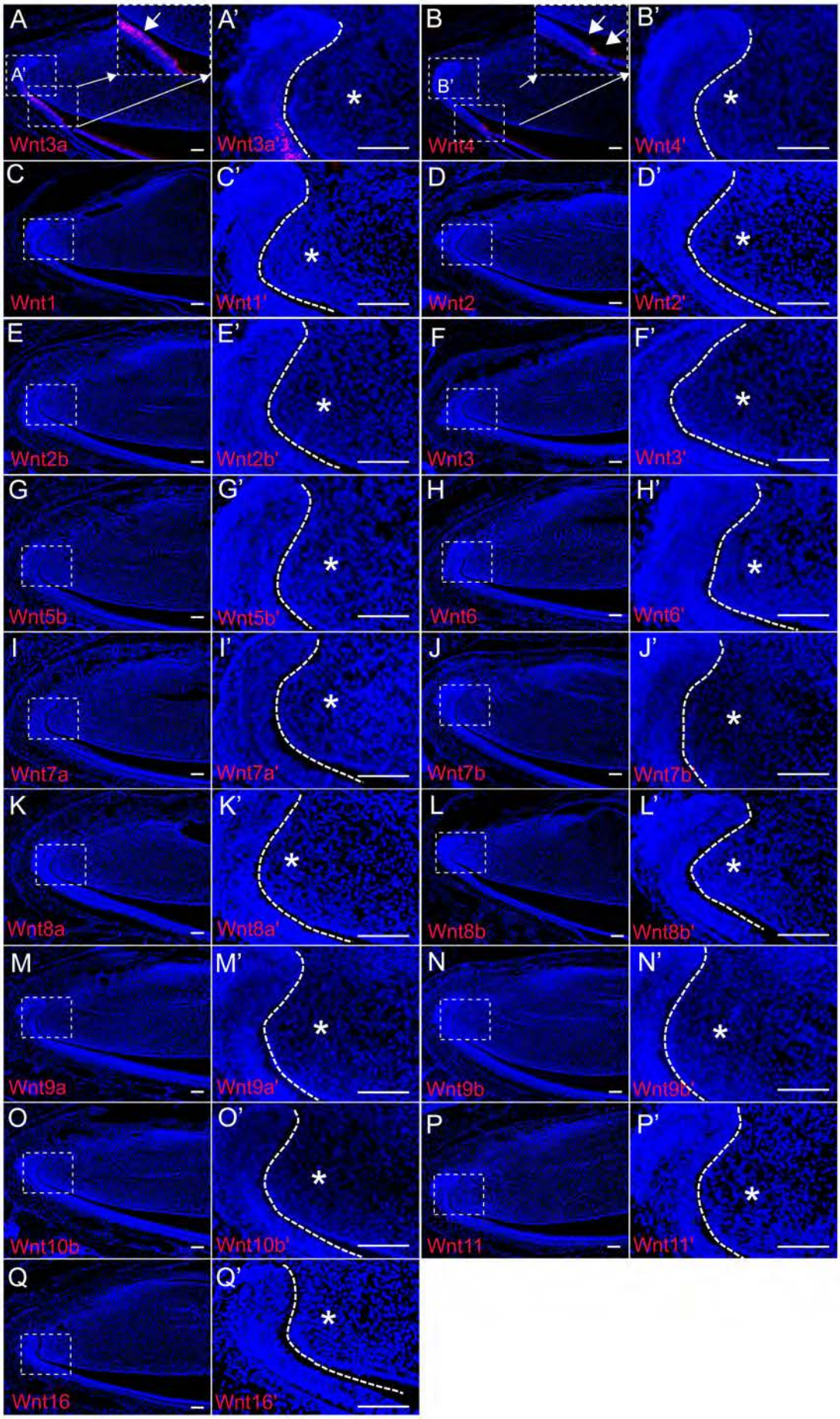

Figure 4-figure supplement 2

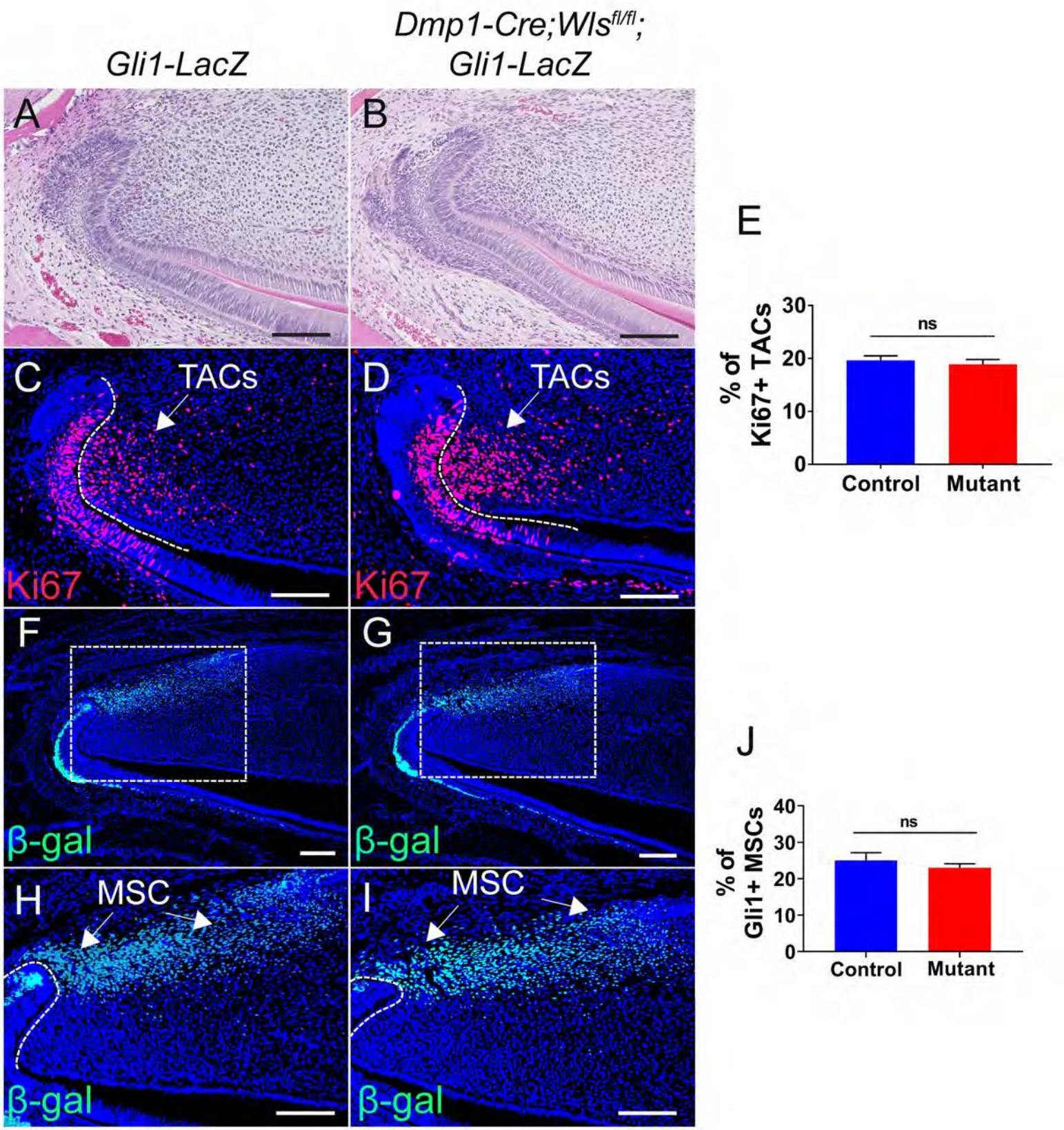

Figure 4-figure supplement 3

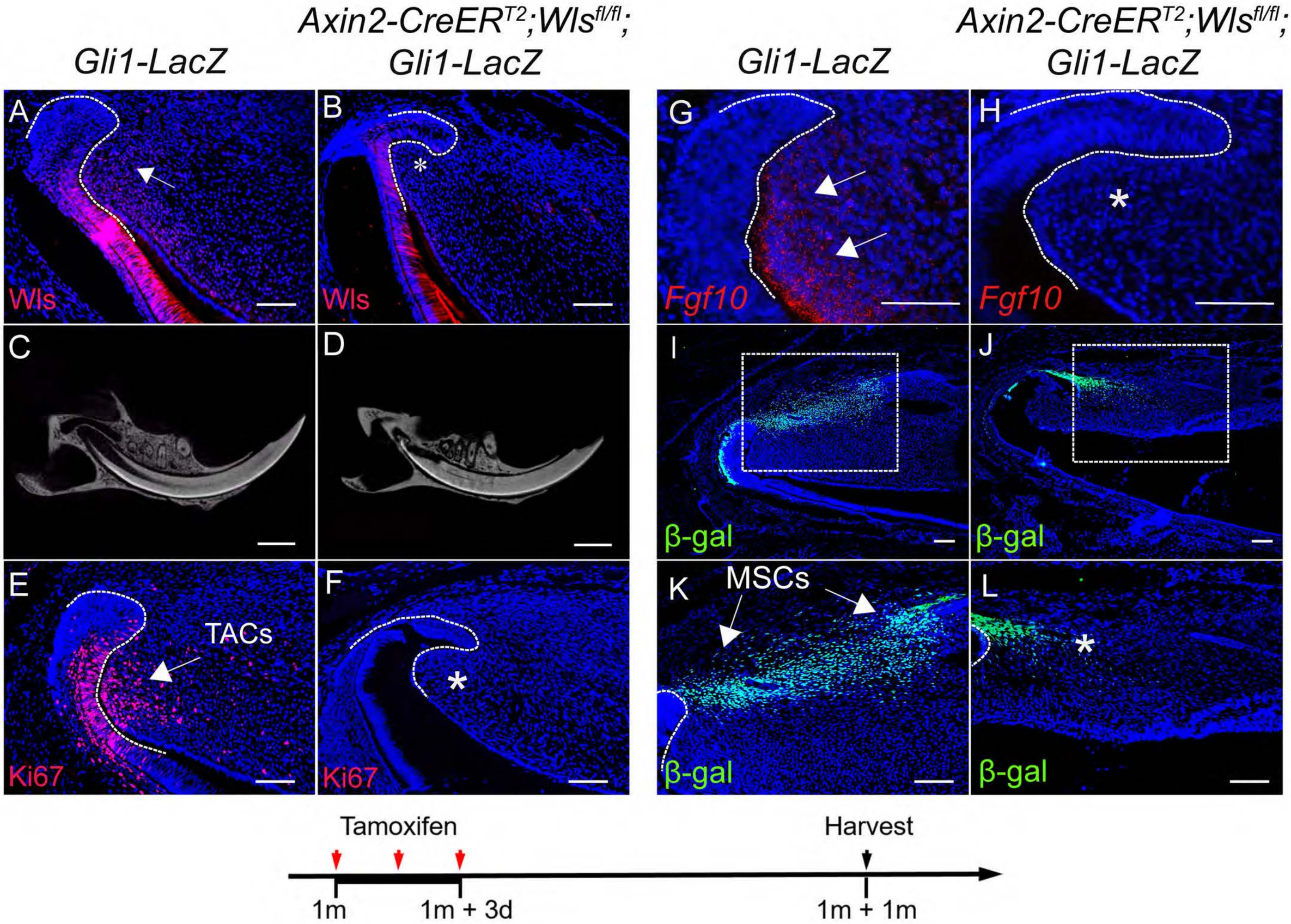

Figure 4-figure supplement 4

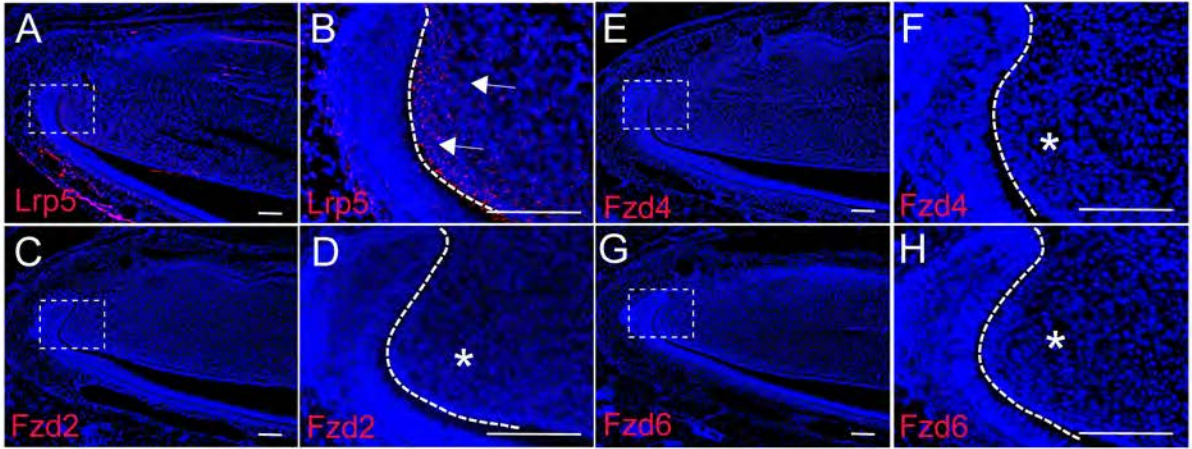

Figure 5

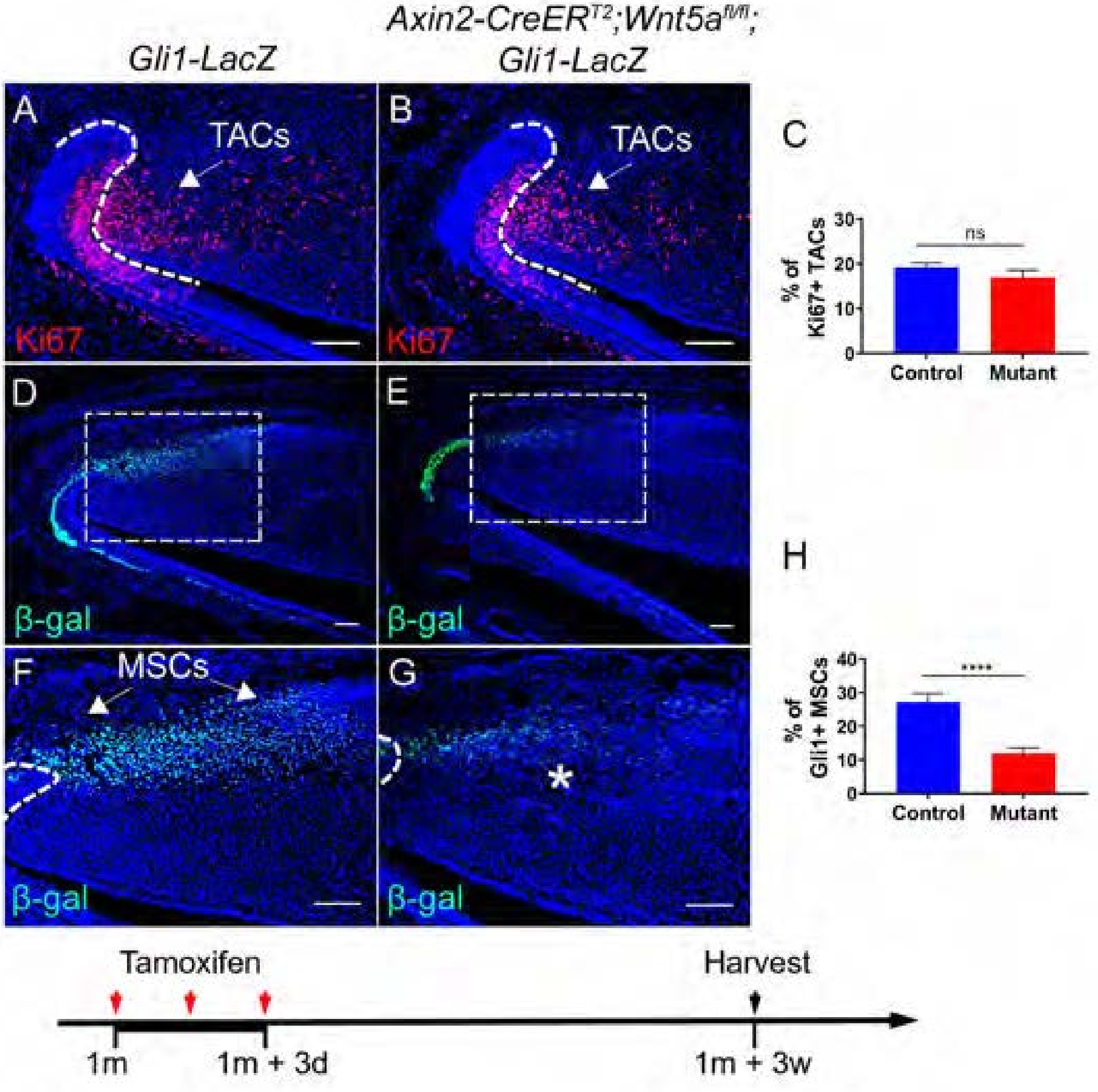
Gli1-LacZ
Axin2-CreER^{T2};Wnt5a$^{fl/fl}$;
Gli1-LacZ
A
TACs
Ki67
B
TACs
Ki67
C
% of Ki67+ TACs
30
20
10
0
ns
Control
Mutant
D
β-gal
E
β-gal
H
% of Gli1+ MSCs
40
30
20
10
0
****
Control
Mutant
F
MSCs
β-gal
G
*
β-gal
Tamoxifen
Harvest
1m
1m + 3d
1m + 3w

Figure 5-figure supplement 1

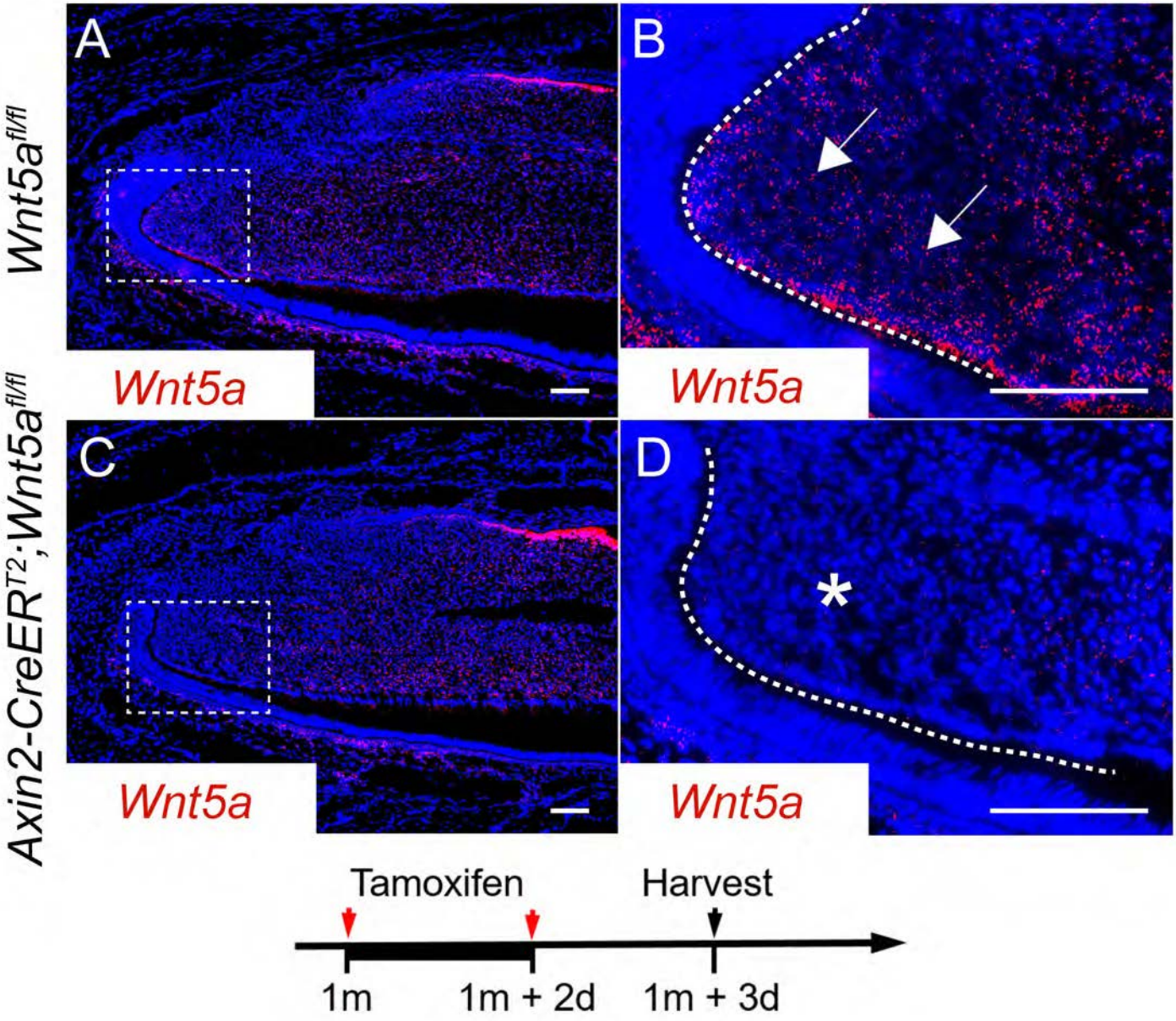

Figure 5-figure supplement 2

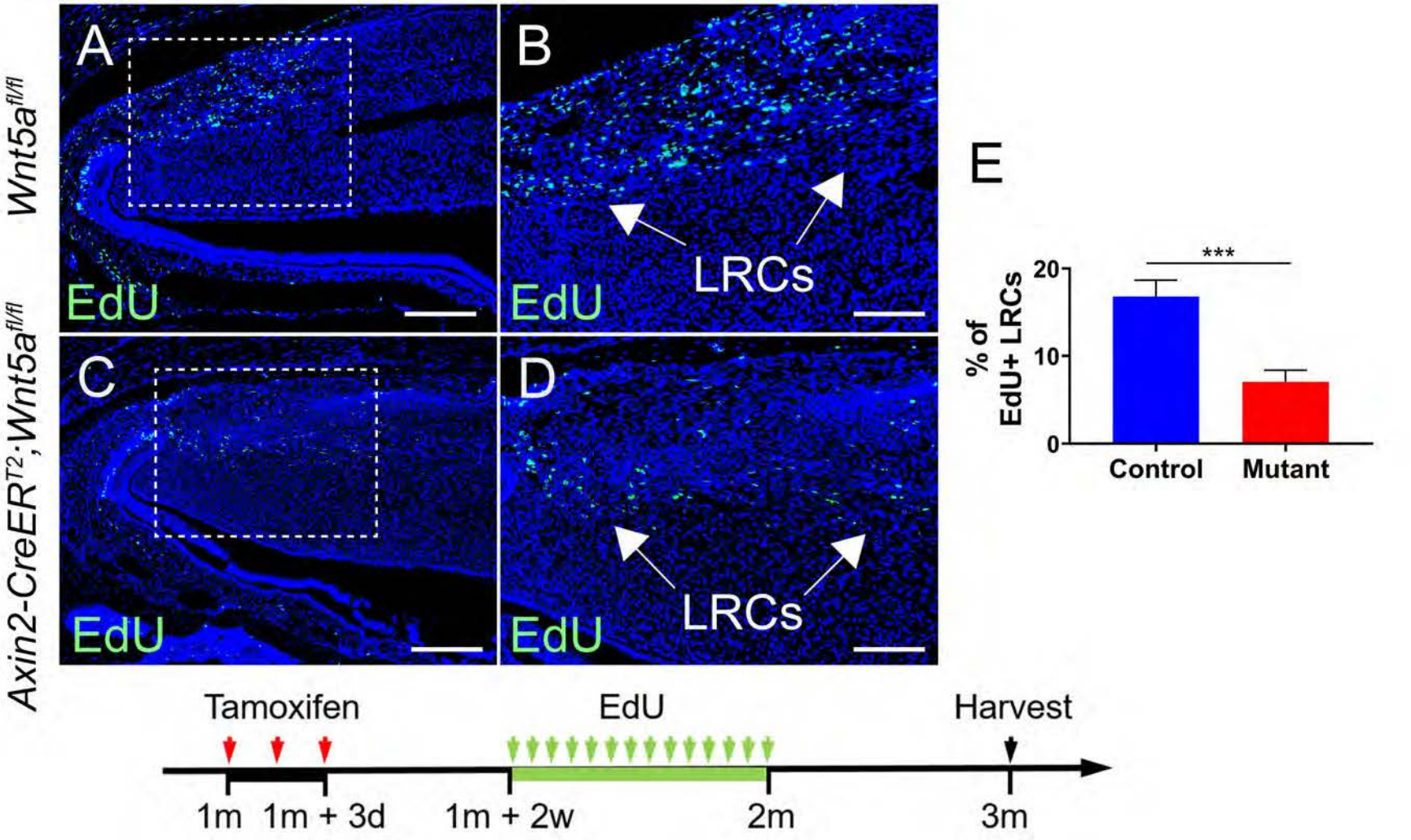

Figure 5-figure supplement 3

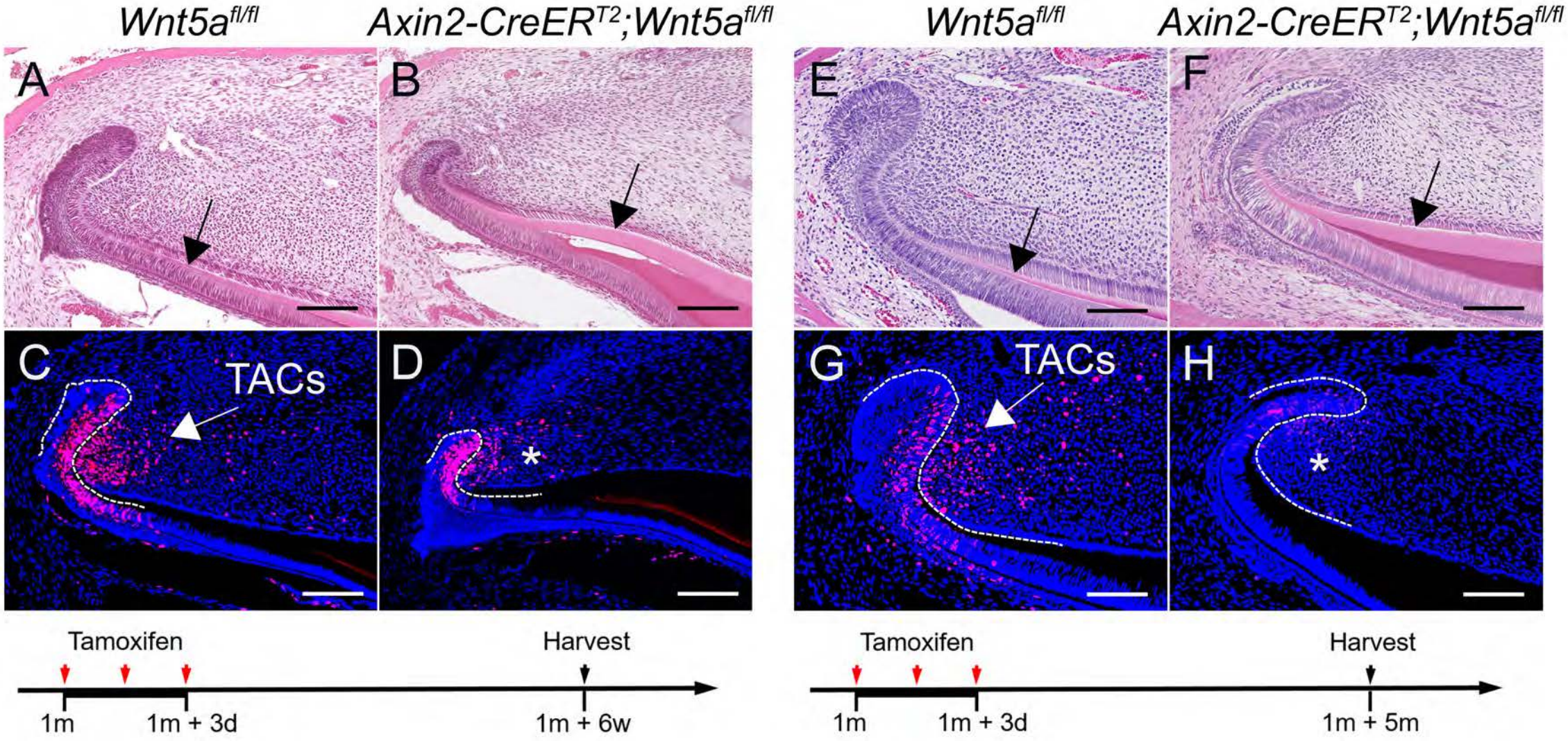

Figure 6

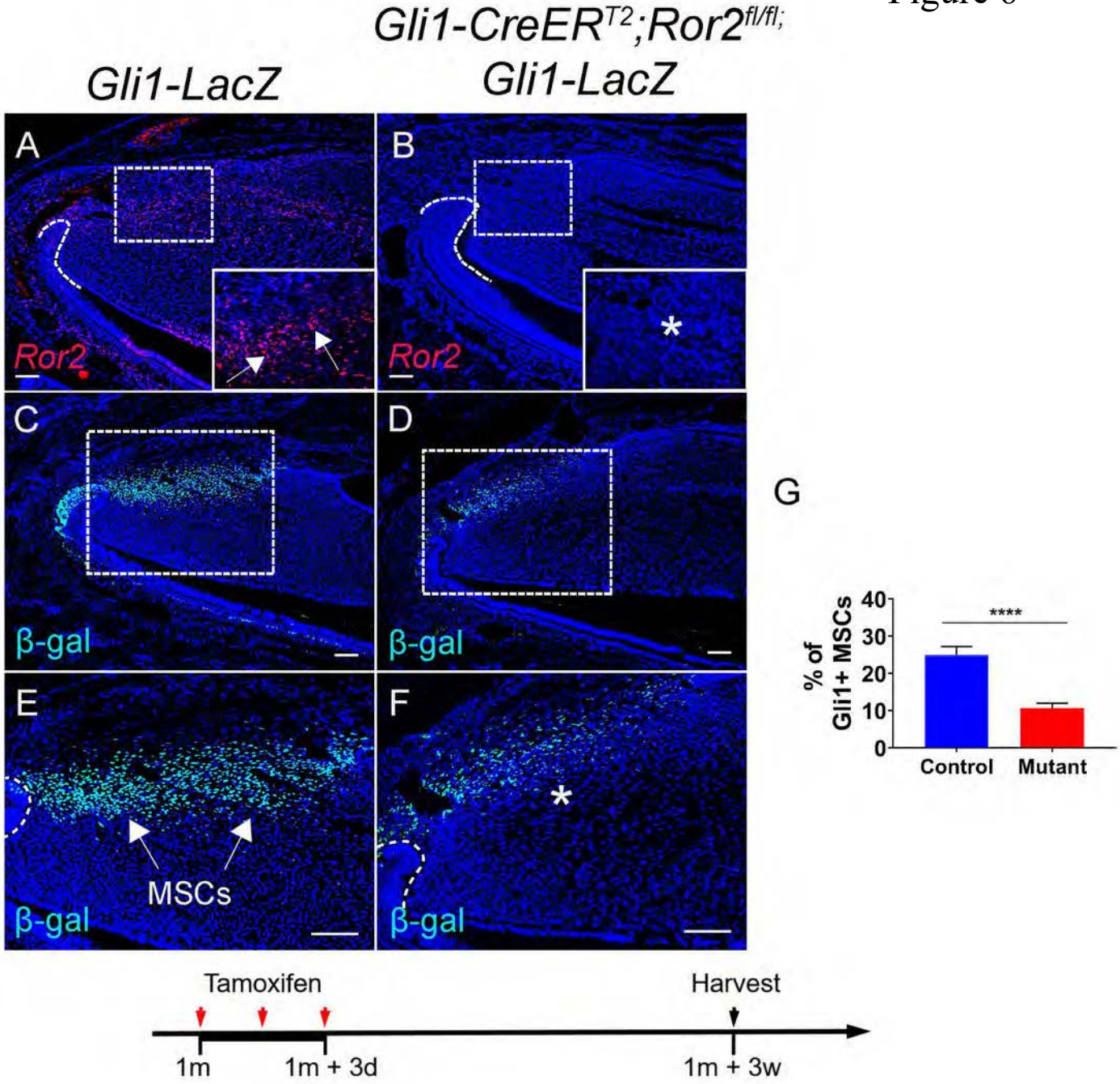
Gli1-LacZ
Gli1-CreER^{T2};Ror2$^{fl/fl;}$ Gli1-LacZ
A
B
Ror2
Ror2
*
C
D
β-gal
β-gal
E
F
MSCs
*
β-gal
β-gal
G
% of Gli1+ MSCs
40
30
20
10
0
****
Control
Mutant
Tamoxifen
Harvest
1m
1m + 3d
1m + 3w

Figure 6-figure supplement 1

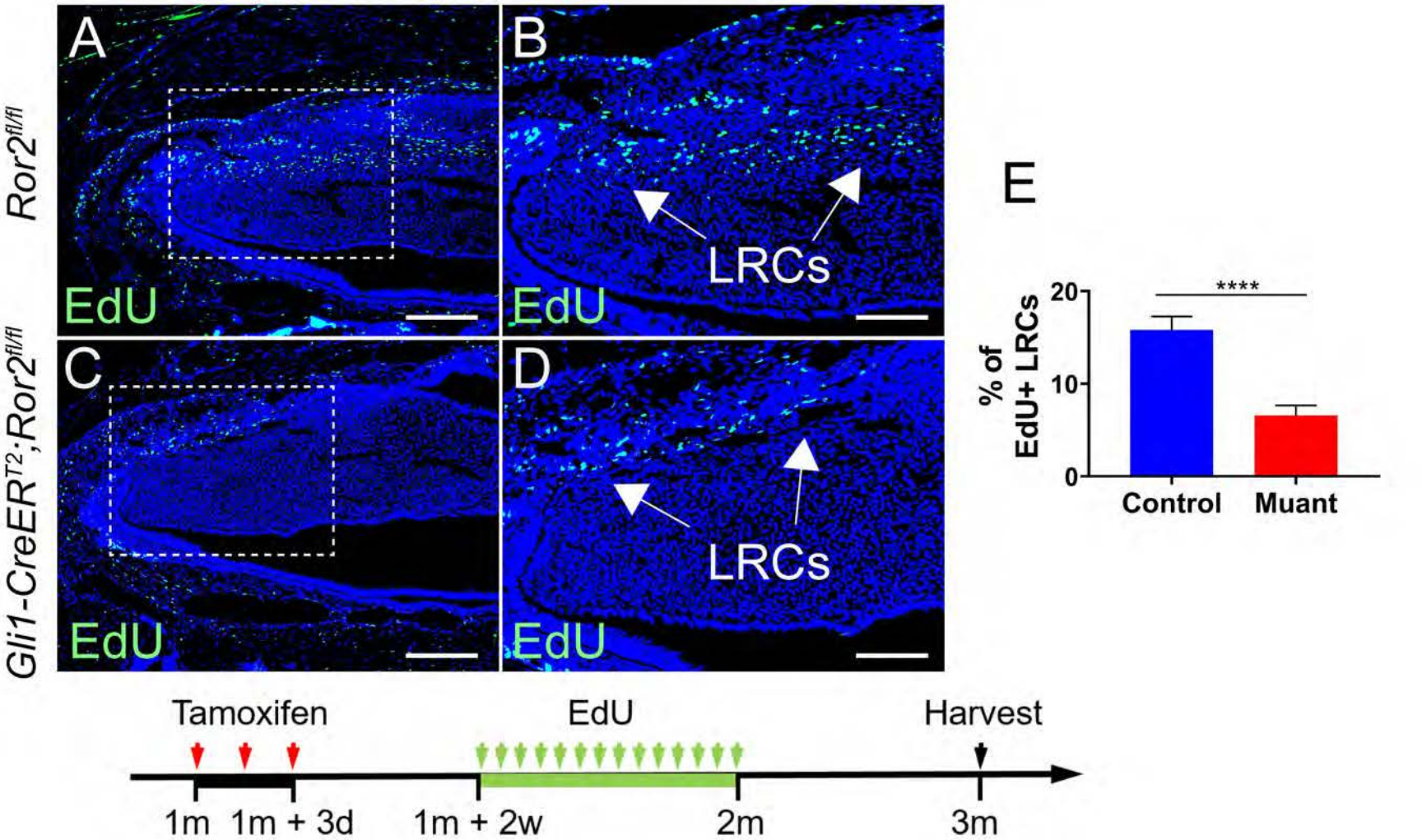

Figure 7

Neurovascular bundle
Dental pulp
Epithelium
Dentin
Enamel
Mesenchymal stem cells (MSCs)
Transit amplifying cells (TACs)